DOE/NASA/1040-79/6
NASA TM-79103

LOW-POWER BASELINE TEST RESULTS FOR THE GPU 3 STIRLING ENGINE

Lanny G. Thieme
National Aeronautics and Space Administration
Lewis Research Center

(NASA-TM-79103) LOW-POWER BASELINE TEST RESULTS FOR THE GPU 3 STIRLING ENGINE Final Report (NASA) 68 p HC E04/MF A01 CSCL 10E

N79-27023

Unclas
G3/85 28628

April 1979

Prepared for
U.S. DEPARTMENT OF ENERGY
Office of Conservation and Solar Applications
Division of Transportation Energy Conservation

DOE/NASA/1040-79/6
NASA TM-79103

LOW-POWER BASELINE TEST RESULTS FOR THE GPU 3 STIRLING ENGINE

Lanny G. Thieme
National Aeronautics and Space Administration
Lewis Research Center
Cleveland, Ohio 44135

April 1979

Prepared for
U. S. DEPARTMENT OF ENERGY
Office of Conservation and Solar Applications
Division of Transportation Energy Conservation
Washington, D. C. 20545
Under Interagency Agreement EC-77-A-31-1040

SUMMARY

In support of the Department of Energy's Stirling Engine Highway Vehicle Systems Program, the NASA Lewis Research Center has converted a 7.5-kilowatt (10-hp) Stirling engine to a research configuration in order to obtain data for validating Stirling-cycle computer simulations. The engine was originally built by General Motors Research Laboratories for the U.S. Army in 1965 as part of a 3-kilowatt engine-generator set that was designated the GPU 3 (Ground Power Unit 3).

Baseline tests were run to map the engine over a range of heater-tube gas temperatures, mean compression-space pressures, and engine speeds with both helium and hydrogen as the working fluid. Tests were limited to the lower power levels because the original alternator and a resistance load bank were used and they were not capable of absorbing the full engine output power.

Test results show that engine output and engine efficiency increased with increasing pressure level. However, the relative gain in power and, particularly, the relative gain in efficiency decreased as pressure increased. The maximum efficiency for a given pressure level was obtained at intermediate speeds. Flow losses caused the efficiency to decrease at high speeds, and conduction losses caused it to decrease at low speeds.

The hydrogen power curves were more linear with speed than were the corresponding helium curves - an indication of the lower flow losses associated with hydrogen. The maximum power obtained with hydrogen was 4.48 kilowatts (6.0 hp) at 4.1 megapascals (600 psi) mean compression-space pressure; the maximum power output with helium was 3.92 kilowatts (5.25 hp) at 6.9 megapascals (1000 psi).

E-9927

INTRODUCTION

This work was done in support of the U.S. Department of Energy's (DOE) Stirling Engine Highway Vehicle Systems Program. The NASA Lewis Research Center, through Interagency Agreement EC-77-A-31-1040 with DOE, is responsible for management of the project under the programmatic direction of the DOE Division of Transportation Energy Conservation.

As part of this effort, Lewis obtained and restored to operating condition a 7.5-kilowatt (10-hp), single-cylinder, rhombic-drive Stirling engine. The engine was originally built by General Motors Research Laboratories for the

U.S. Army in 1965 as part of a 3-kilowatt engine-generator set that was designated the GPU 3 (Ground Power Unit 3).

The GPU 3 Stirling engine test program at Lewis has three objectives:

(1) To obtain and publish detailed engine performance data (These data, along with the engine dimensions necessary for modeling, should assist in the development of Stirling engine simulation techniques.)

(2) To validate, document, and publish a NASA Lewis Stirling computer model

(3) To provide a test bed for evaluating new component concepts that evolve from supporting Stirling-engine technology activities

The engine was converted to a research configuration so that the necessary data could be obtained. The engine-driven accessories from the original GPU 3 package were removed and extensive instrumentation was added. Baseline tests were then run to map the engine over a range of heater-tube gas temperatures, mean compression-space pressures, and engine speeds with both helium and hydrogen as the working fluid. Tests, however, were limited to the lower power levels because the original alternator and a resistance load bank were used and they were not capable of absorbing the full engine output power.

This report presents results from these tests plotted as curves of engine output and brake specific fuel consumption as functions of engine speed, mean compression-space pressure, and heater-tube gas temperature. An instrumentation system for measuring indicated work is also described and preliminary results are presented.

The engine dimensions necessary for modeling, as well as the results of volume measurements and steady-state flow tests, are presented in the appendixes. The detailed data taken during these baseline tests are included on microfiche as part of this report. A sample data point and the format information needed to interpret the data are given in the appendixes.

These data have been used to make the initial direct comparisons with the Lewis computer simulation predictions. The simulation code is described in references 1 and 2. Results of the simulation comparisons with the test data are given in reference 2.

The tests and results covered in this report are also briefly described in reference 3.

APPARATUS AND PROCEDURE

GPU 3 STIRLING ENGINE

Description and Background

The GPU 3 Stirling engine as recently tested at Lewis is shown in figure 1. The engine was obtained from the U.S. Army Mobility Equipment Research and Development Center (MERDC) at Fort Belvoir, Virginia. A second, identical engine was also obtained through a loan from the Smithsonian Institution. This second engine has so far been used as a source of spare parts for the Army engine. Both engines were originally part of identical 3-kilowatt engine-generator sets built by General Motors Research Laboratories in 1965 for the U.S. Army. These units were completely self-contained and capable of operating with a variety of fuels over a broad range of ambient conditions. They were designed to use hydrogen as the working fluid. The GPU 3 engine is a single-cylinder, displacer engine with a rhombic drive and sliding rod seals. It is capable of producing a maximum engine output of approximately 7.5 kilowatts (10 hp) with hydrogen working fluid at 6.9 megapascals (1000 psi) mean compression-space pressure. The piston swept volume is 120 cubic centimeters (7.3 in.^{3}).

The engine obtained from Fort Belvoir was initially torn down and restored to operating condition. It was then tested as part of the original GPU 3 with only those changes that were necessary to make the unit operable. Tests were run with both hydrogen and helium as the working fluid at various pressures and at the design heater-tube gas temperature of 675° C (1250° F) and an engine speed of 3000 rpm. Comparisons were made with data taken by the Army in 1966. These results and a description of the original GPU 3 engine components and systems are given in reference 4.

Conversion to Research Engine

The GPU 3 engine is used primarily to provide data for modifying and validating Stirling-cycle simulation techniques. The Lewis simulation that will directly make use of these data is described in references 1 and 2. The following changes were made to convert the engine to a research configuration so that the required data could be obtained. Where necessary, new parts (power piston, cooler-regenerator cartridges, displacer shaft) were made and others (fuel nozzle) were reworked to allow successful operation. Dimensional and volume mea-

surements were completed to determine the engine dimensions necessary for modeling. Steady-state flow tests were made on the coolers, the regenerators, the cooler-regenerator cartridges, and the entire heater head in order to determine pressure-drop-versus-mass-flow-rate characteristics. The engine dimensions, volume measurements, and flow tests are described in appendixes A, B, and C, respectively. The engine-driven accessories were removed, with the exception of the oil system. Air, water, fuel, and working fluid were provided from the facility support systems. These facility systems are discussed in the section TEST SETUP. The control system of the original GPU 3 was replaced with manual controls.

Finally, instrumentation was added to the engine and facility systems in order to obtain an energy balance, engine temperature profiles, conduction losses, working-space gas temperatures and dynamic pressures and to attempt to measure indicated work. Instrumentation in the facility systems is discussed in the section TEST SETUP. Instrumentation on the engine included 32 thermocouples on the cylinder assembly for measuring surface temperatures; 15 thermocouples on the preheater, including three for measuring exhaust temperature; six thermocouple probes for measuring working-fluid temperatures at various locations; three miniature pressure transducers in the expansion, compression, and buffer spaces; and a shaft encoder to measure crankshaft angle. An instrumentation list and sketches showing measurement locations are included in appendix D.

TEST SETUP

A schematic diagram of the GPU 3 test setup is shown in figure 2. Facility support systems shown include fuel, air, cooling water, oil, and working fluid. Also shown are the alternator and the resistance load bank that were used to absorb the engine output. Numbers by the instrumentation symbols refer to the item numbers in table III.

The fuel system included two external tanks that were pressurized with nitrogen: One tank, the startup tank, was used to supply fuel during engine startup and while a data point was being established. The second tank, the run tank, was used while data were being taken. Its weight was recorded before and after each data point to determine the amount of fuel used.

The air system consisted of two separate lines to supply nozzle air for fuel atomization and combustion air to the preheater inlet. Mass flow, pressure, and temperature were measured in each line. Each supply could be controlled separately to the desired pressure or flow.

City water was used to supply cooling water to the engine and was not recycled through the engine. The water system consisted of three separate circuits. The main circuit provided flow through the coolers and around the cylinder. Separate lines cooled the buffer space and the fuel nozzle. Inlet water temperature was measured for the total flow. The flow rate and the temperature rise from the outlet to the inlet were recorded for each circuit as well as for the total flow. Total water flow rate could be set to the desired value, but water inlet temperature was not controlled.

The oil pump remained engine driven as it was in the original GPU 3. The oil was cooled by a separate oil cooler and then recirculated through the engine. Flow rate, pressure, inlet temperature to the engine, and temperature rise from the outlet to the inlet were measured for the oil circuit.

The system to provide the working fluid included an external gas-supply panel connected to helium and hydrogen bottles so that it could supply either working fluid to the pressurization system. The pressurization system then supplied the working fluid to the engine. Mean pressure was measured in both the compression and buffer spaces of the engine.

The original GPU 3 alternator and a separate resistance load bank were used to absorb the engine output power. In the GPU 3 engine-generator set, the alternator output voltage was regulated to a constant 30 volts at design conditions. This voltage regulator was removed and a fixed 28-volt field voltage was used to increase the alternator capacity. The alternator was calibrated to define its efficiency at various speeds and output voltages. The original GPU 3 package was designed for a 3-kilowatt output. Although the maximum possible alternator output was increased for these tests, the alternator was still not capable of the maximum engine output. Thus, these tests were limited by the method of power absorption. Primarily, the restrictions were maximum alternator current and load bank capacity.

The GPU 3 test setup is shown in figure 3. The engine and facility systems just described are shown on the right half of the figure. The left half shows the signal conditioning equipment and the data recording systems. Steady-state data were recorded and printed out on a data logger. Dynamic data were taken with both an oscillograph recorder and an oscilloscope.

TEST PROCEDURE

The desired test matrix range for both the helium and hydrogen runs was as follows: mean compression-space pressure, 1.4 to 6.9 megapascals (200 to 1000 psi); heater-tube gas temperature, 595° to 705° C (1100° to 1300° F); and engine speed, 1000 to 3500 rpm. The actual range of the tests was determined by the limitations due to the alternator and resistance load bank. The heater-tube gas temperature was measured with thermocouple probes installed inside three of the 40 heater tubes and spaced circumferentially around the heater head. The maximum reading of these three thermocouples was controlled to the desired temperature by adjusting the fuel flow with a needle valve. The cooling-water inlet temperature was not controlled and varied about 5.5 degrees Celsius (10 deg F) over the series of tests. However, this temperature did remain constant for any given test run.

On each engine startup, cooling-water flow was first provided to the engine, and the mean compression-space pressure was set at approximately 1.7 megapascals (250 psi). Combustion was then begun with No. 1 diesel fuel from the startup fuel tank. When the heater-tube gas temperature reached 675° C (1250° F), the starting cable was pulled to rotate the crankshaft and move the pistons. The engine would then normally sustain operation. A reference point of 705° C (1300° F) heater-tube gas temperature, no load, and 3000-rpm engine speed was established to verify proper engine operation and to allow the engine to reach operating temperatures.

Generally, one curve at constant mean compression-space pressure, heater-tube gas temperature, and cooling-water flow was run after each engine startup. The curve consisted of data points taken at engine speeds varying by 500-rpm intervals. At each point, the resistance load was adjusted to establish the desired speed. The combustion airflow was set to maintain an approximately constant air-fuel ratio. After proper conditions were reached, the fuel run tank was valved to the engine. These conditions were then maintained for 15 minutes. All steady-state data were recorded three times and dynamic data once during this period. The startup fuel tank was then again valved to the engine and the next data point established. The fuel flow was determined from the initial and final weights of the fuel run tank. This procedure was repeated for each data point.

RESULTS AND DISCUSSION

The influence of mean compression-space pressure and heater-tube gas temperature on engine output and brake specific fuel consumption (bsfc) are shown in figures 4 to 9. All curves are plotted with engine speed as the abscissa. Examples of energy balances obtained on the engine are given in figures 10 and 11. All detailed data taken during these tests are included on microfiche in the back of this report. Appendixes D, E, and F give all the information needed to understand the microfiched data. A sample data point is included in appendix F.

PRESSURE EFFECTS ON ENGINE PERFORMANCE WITH HELIUM

The effects of mean compression-space pressure and engine speed on engine performance at constant heater-tube gas temperature are illustrated in figures 4 and 5 for helium working fluid. Engine output and bsfc versus engine speed are shown as a function of pressure at 650° C (1200° F) and 705° C (1300° F) heater-tube gas temperatures, respectively. Of the three steady-state data scans taken at each operating condition, two were reduced and plotted. When both scans gave approximately the same results, only one symbol is shown plotted for that condition. The engine output was determined by measuring the output power of the alternator and dividing this power by the alternator efficiency.

The incomplete curves at the higher pressure levels indicate the limiting current capacity of the alternator and load bank. This limit established the minimum speed at which the engine could be operated for a given pressure. Also, because of this current limitation, the engine could not be operated at 6.9 megapascals (1000 psi) at 705° C (1300° F) heater-tube gas temperature. Finally, the maximum speed for the 1.4-megapascal (200-psi) curve at 705° C (1300° F) heater-tube gas temperature was only 2500 rpm. This was the highest speed for which the engine could sustain operation for this pressure level with helium.

For a constant pressure, the engine output and brake thermal efficiency tended to decrease at the higher speeds. This was primarily due to the increasing flow losses through the heat exchangers. This effect was substantiated by the computer simulation predictions. At the lower speeds, the conduction and other fixed heat losses became a significant percentage of the heat input and caused the efficiency to decrease. Therefore, the efficiency tended to

maximize (minimum bsfc) at some intermediate speed, as shown in figures 4 and 5.

For a given speed, the engine output and efficiency both increased with increasing pressure level. The increasing output was due to more mass in the cycle, and the increasing efficiency was due to the smaller percentage that the conduction and other fixed heat losses and the mechanical losses contributed to the heat input. These effects on the efficiency are shown with the energy balances. However, the spacing between the curves shows that, as the pressure increased, the relative gain in power and particularly the relative gain in efficiency decreased. Part of this decreasing efficiency gain can be attributed to the diminishing effect had by the percentage of heat losses and the mechanical losses relative to the heat input as the pressure increased. Thus, this effect caused the efficiency to increase with pressure as mentioned previously, but also to do so at a decreasing rate. In addition, as pressure increased, both power and efficiency appeared to be affected by heat-transfer limitations at the cold end of the engine. During testing, the compression-space gas temperature was observed to increase with pressure at a fixed speed. For example, the compression-space gas temperature rose from 91° C (195° F) at 2.8 megapascals (400 psi) and 3000 rpm to 119° C (247° F) at 6.9 megapascals (1000 psi) and 3000 rpm. Thus, the Carnot efficiency based on the gas temperatures was less for the higher pressure levels although the heater-tube gas temperature and the cooling-water inlet temperature remained the same.

The maximum power obtained with helium was 3.92 kilowatts (5.25 hp) at a mean compression-space pressure of 6.9 megapascals (1000 psi). The minimum bsfc measured was 602 g/kW · hr (0.99 lb/hp · hr), which corresponds to 13.9 percent brake thermal efficiency.

PRESSURE EFFECTS ON ENGINE PERFORMANCE WITH HYDROGEN

The effects of mean compression-space pressure and engine speed on engine performance at constant heater-tube gas temperature are shown in figure 6 for hydrogen working fluid. Engine output and bsfc versus engine speed are shown as a function of pressure at 705° C (1300° F) heater-tube gas temperature. These data were taken over a smaller pressure range than were the helium data because the higher power output with hydrogen at a given pressure caused the limiting alternator values to be reached at a lower pressure level.

The hydrogen power curves are more linear with speed and peak out at a much higher speed than do the corresponding helium curves. Also, the bsfc

curves are much flatter at higher speeds than are those for helium. These are indications of the lower flow losses associated with hydrogen.

The maximum engine output with hydrogen was 4.48 kilowatts (6.0 hp) at 4.1 megapascals (600 psi) and 3500 rpm. The minimum bsfc was 492 g/kW · hr (0.81 lb/hp · hr) at 2.8 megapascals (400 psi) and 2500 rpm. This corresponds to a brake thermal efficiency of 16.9 percent.

EFFECTS OF HEATER-TUBE GAS TEMPERATURE ON ENGINE PERFORMANCE

Test data were taken to determine the effect of varying heater-tube gas temperature. For a constant mean compression-space pressure, tests were run at heater-tube gas temperatures of 595° C, 650° C, and 705° C (1100° F, 1200° F, and 1300° F). Figures 7 and 8 show engine output and bsfc versus engine speed at these temperatures for helium at 2.8 and 5.5 megapascals (400 and 800 psi), respectively. Figure 9 shows the same for hydrogen at 2.8 megapascals (400 psi). The engine output and efficiency both increased with increasing heater-tube gas temperature, as was expected.

ENERGY BALANCES

Two examples of an energy balance on the engine operating with helium are shown in figure 10. Both graphs are for a heater-tube gas temperature of 650° C (1200° F) and an engine speed of 3000 rpm. The first is for an engine output of 1.05 kilowatts (1.4 hp) at a mean compression-space pressure of 2.8 megapascals (400 psi); the second is for 3.9 kilowatts (5.2 hp) at 6.9 megapascals (1000 psi). The bar graphs indicate that more than 98 percent of all heat input was accounted for at these two points. More than 93 percent of the input energy was accounted for in most heat balances taken during these tests.

As shown in figure 10, the exhaust losses and the cycle heat rejection to the cooling water accounted for most of the energy losses. The cycle heat rejection was found by measuring the heat flow to the water passing through the coolers and subtracting the conduction losses. The heat loss to the exhaust gas was substantial because of the high air-fuel ratio (about 40 for the points shown in fig. 10). This tended to adversely affect the overall engine efficiencies. In addition, excessive exhaust temperatures exiting the preheater indi-

cated poor preheater performance, which would further decrease the measured efficiencies.

For any given heater temperature, the conduction losses through the engine were approximately constant. Also, the radiation and convection losses and the nozzle water losses increased much more slowly with pressure than did the heat input from the fuel. Consequently, these losses accounted for a greater percentage of the heat input at low pressure levels, where the engine output was low. The bar graphs indicate that the percentage of loss due to conduction, radiation and convection, and nozzle water losses at 2.8 megapascals (400 psi) was almost double that at 6.9 megapascals (1000 psi). Also, the heat to the oil and buffer water can be taken as an indication of the mechanical losses in the engine. The graphs show that for a constant speed these losses, too, were a larger percentage of the heat input at the lower pressures and were especially significant when compared with the engine output.

Energy balances as a function of engine speed for helium working fluid are shown in figure 11 for a heater-tube gas temperature of 650° C (1200° F) and a mean compression-space pressure of 2.8 megapascals (400 psi). To determine the actual magnitude of the losses, refer to the engine output graphed in figure 4. For these balances, more than 95 percent of the energy was accounted for at each point although a value slightly over 100 percent was measured at 1000 rpm.

The conduction, radiation and convection, and nozzle water losses were approximately constant over the speed range for any given heater-tube gas temperature and pressure. Because the heat input from the fuel increased with speed, these losses represented a greater percentage of the heat input at the lower speeds, as is verified by the energy balance. As a result the engine efficiency began to decrease at the lower speeds, as indicated previously in the bsfc curves and shown in the engine output curve of the energy balance.

The heat to the oil and buffer water was nearly a constant percentage of the heat input throughout the speed range. It became particularly significant at high speed for these helium curves, where flow losses caused the engine output to decrease substantially.

The cycle heat rejection and exhaust losses again accounted for most of the heat loss. The exhaust losses varied because of a fluctuating air-fuel ratio that was especially high at the lowest speed. For comparisons with the computer simulation, the exhaust losses and other burner losses were subtracted from the heat input from the fuel to obtain the heat input into the engine. Thus, maintain-

ing a constant air-fuel ratio became less important for computer validation purposes as long as the exhaust losses could be accounted for.

INDICATED-WORK MEASUREMENT

Description of Measurement System

Initial attempts to determine the indicated work produced by the working fluid in the engine were made by measuring the pressure-volume relationships in the working space. Pressure-volume diagrams were obtained for the expansion and compression spaces; and the indicated work was expansion work minus compression work. A pressure-volume diagram was also obtained for the buffer space and compared with the heat rejection to the buffer cooling water.

The dynamic pressure measurements were made with miniature pressure transducers in the expansion, compression, and buffer spaces. The compression- and buffer-space transducers were approximately flush mounted. The expansion-space transducer was installed at the end of a 0.16-centimeter-(0.063-in.-) inside-diameter tube about 15.2 centimeters (6 in.) long. This tube was then inserted into one of the four oversized heater tubes that led into the expansion space and that were specially modified in the original GPU 3 design to accept instrumentation. The necessary volumes were predetermined and referenced from the crankshaft angle. The crankshaft angle was measured with respect to displacer top-dead-center by the shaft-angle encoder shown in figure 12. The encoder was mounted on the accessory drive shaft of the original GPU 3 and was capable of resolving the crankshaft angle to 0.35-degree increments.

The recording system for the pressure-volume measurements is shown in figure 13. The crankshaft-angle signal was input to the module rack located above the switch panel. From this signal, the function generator produced a marker channel that was used to determine the phase angles of the pressure peaks. The marker channel could be recorded on the oscillograph and displayed on the oscilloscope. The volume generator used the crankshaft angle and the associated volumes stored inside the volume generator module to produce the volume signal for each of the three spaces.

The switch panel received the pressure and volume signals as input. The switching arrangement was used to select which combination of pressure and volume to display on the scope. The normal procedure was to photograph each of the three pressure-volume diagrams from the scope for each operating con-

dition. A planimeter was then used to determine the area inside each diagram and, thus, the work.

The indicated work was also measured from the compression-space pressure versus the total working-space volume (expansion plus compression volume). This pressure-volume diagram could be displayed on the oscilloscope. In addition, the IMEP module, developed at Lewis and shown in figure 13, numerically integrated the pressure-volume diagram to obtain the work in terms of indicated mean effective pressure (IMEP). To perform the integration, the module used the compression-space pressure and the derivative of the total working-space volume stored in its memory as a function of crankshaft angle. The value of IMEP calculated and displayed was an average value obtained over 100 engine cycles. An IMEP value for each cycle was also available to be recorded on the oscillograph.

IMEP modules will soon be available for determining the work in the individual spaces (expansion, compression, and buffer), and other modules will be available to determine the pressure maximums and minimums and their phase angles. Reference 5 provides more information on this type of instrumentation system.

Preliminary Results of Indicated-Work Measurements

Several of the preliminary results of indicated-work measurements are shown in figures 14 and 15. Figure 14 illustrates the pressure-volume diagrams for the expansion and compression spaces for helium working fluid at a heater-tube gas temperature of 650° C (1200° F), a mean compression-space pressure of 2.8 megapascals (400 psi), and an engine speed of 3000 rpm. Figure 15 shows the results at the same operating conditions for hydrogen working fluid.

Each diagram gives the indicated work, the pressure swing, and the location of the 90-degree intervals with displacer top-dead-center as a reference. These 90-degree locations indicate that the expansion-space diagram was being traced clockwise (positive work) and that the compression-space diagram was being traced counterclockwise (negative work), as would be expected. Absolute values of the pressure maximums and minimums could not be determined because of zero shifts of the pressure signals caused by temperature effects on the miniature transducers.

The helium pressure-volume diagrams yielded an indicated power of 2.31 kilowatts (3.10 hp). The indicated power from the heat balance was 2.28 kilo-

watts (3.05 hp), as calculated from the heat into the gas minus the cycle heat rejection. The heat into the gas was found by using the heat input from the fuel and subtracting the exhaust, radiation and convection, nozzle water, and conduction losses. The cycle heat rejection is defined in the section ENERGY BALANCES. The engine output (brake power) was 1.05 kilowatts (1.4 hp).

The hydrogen pressure-volume diagrams yielded an indicated power of 3.47 kilowatts (4.65 hp). The indicated power from the heat balance was 3.46 kilowatts (4.63 hp). Another method of comparing the hydrogen diagrams was to use the mechanical loss curves derived from General Motors motoring tests of the GPU engine with hydrogen as the working fluid. Motoring curves for helium were not available. The hydrogen motoring data are given in reference 6. The mechanical losses for this operating condition from the motoring data were approximately 1.16 kilowatts (1.55 hp). Adding this to the Lewis measured engine output of 2.41 kilowatts (3.23 hp) yielded an indicated power of 3.57 kilowatts (4.78 hp). Thus, the results from each method for these operating conditions are in agreement and appear to be reasonable values for the indicated work.

The overall results obtained are preliminary and do not agree as well for every point as for those that are shown. There are problems associated with sensitivity changes of the pressure transducers due to temperature effects and with accurately locating a crankshaft-angle reference. Work is proceeding to alleviate these problems in future testing. Also, mechanical losses will be determined by motoring tests to better ascertain the accuracy of the indicated-work results.

CONCLUDING REMARKS

The data from these tests are being compared directly with the Lewis Stirling-cycle simulation code. These comparisons are being made to aid in determining the primary reasons why predictions and experimental observations differ.

The detailed test data are included on microfiche in the back of this report. It is hoped that making available the combination of detailed test data and the corresponding engine dimensions necessary for modeling will further the development of Stirling-cycle computer simulations. All information needed to understand the microfiched data is included in the appendixes.

Preliminary results from the indicated-work measurement system were satisfactory and indicate that this work should serve as a good basis for

further refining this useful measurement technique. The uncertainty, in comparison with simulation predictions of engine output, associated with accurately specifying the mechanical losses could be eliminated by directly measuring the indicated power developed by the engine.

Future test work with the GPU 3 engine will include mapping the engine at the higher power levels with a dynamometer. Motoring tests will also be run to aid in determining the mechanical losses.

SUMMARY OF RESULTS

The GPU 3 Stirling engine has been converted to a research configuration. The engine was mapped over a limited range at heater-tube gas temperatures from 595° to 705° C (1100° to 1300° F), mean compression-space pressures from 1.4 to 6.9 megapascals (200 to 1000 psi), and engine speeds from 1000 to 3500 rpm with both hydrogen and helium as the working fluid. The major results obtained from these tests are as follows:

1. Engine output and engine efficiency increased with increasing pressure level. However, the relative gain in power and, particularly, the relative gain in efficiency decreased as pressure increased.

2. The maximum efficiency (minimum brake specific fuel consumption (bsfc)) for a given pressure level was obtained at intermediate speeds. Flow losses caused the efficiency to decrease at high speeds, and conduction losses caused it to decrease at low speeds.

3. The hydrogen power curves were more linear with speed than were the corresponding helium curves - an indication of the lower flow losses associated with hydrogen.

4. An instrumentation system was developed to measure the indicated work of the engine. This measurement will allow direct comparison with the indicated-work predicted by the computer simulation. Thus, accurate knowledge of the engine mechanical losses will not be necessary for the engine output comparison.

5. The maximum power obtained with hydrogen was 4.48 kilowatts (6.0 hp) at 4.1 megapascals (600 psi) mean compression-space pressure and 705° C (1300° F) heater-tube gas temperature. The minimum bsfc was 492 g/kW · hr (0.81 lb/hp · hr).

6. The maximum power obtained with helium was 3.92 kilowatts (5.25 hp) at 6.9 megapascals (1000 psi) mean compression-space pressure and 650° C (1200° F) heater-tube gas temperature. The minimum bsfc was 602 g/kW · hr (0.99 lb/hp · hr).

APPENDIX A

GPU 3 ENGINE DIMENSIONS AND PARAMETERS

This appendix gives the GPU 3 Stirling-engine dimensions and parameters that are necessary to model the engine for a computer simulation. The primary engine dimensions as they apply to the test data reported herein are listed in table I. Table II gives a breakdown of the various dead volumes in the engine. The dimensions needed for calculating heat conduction through the cylinder and regenerator housings are shown in figure 16. Also shown in this figure are the thermocouple locations for these measurements. The dimensions needed for calculating conduction losses through the insulation covers are included in table I.

APPENDIX B

GPU 3 VOLUME MEASUREMENTS

The gas volumes in the working and buffer spaces of the GPU 3 engine were measured by a gas-displacement method. These data were then used to verify the volumes in the NASA Lewis computer simulation. So that the measurements could be made, an O-ring was first installed around the power piston to prevent leakage from the working space to the buffer space. The power piston was set at top-dead-center to allow measurement of minimum working-space volume and maximum buffer-space volume.

A burrette was connected to the unknown gas volume and to a water reservoir. A known volume of gas was then displaced and the pressure rise measured. A second burrette was installed in the water line to measure the pressure differential ΔP. The unknown gas volume was then found from PV = Constant (Boyles' law). This method was based on that reported in reference 7. The calculation procedure was as follows:

$$P_{initial}V_{initial} = P_{final}V_{final}$$

$$P_{ambient}(V_{unknown} + V_{burrette-initial} + V_{connecting\ tubing}) =$$

$$(P_{ambient} + \Delta P)(V_{unknown} + V_{burrette-final} + V_{connecting\ tubing})$$

where

$$V_{burrette-final} < V_{burrette-initial}$$

Typical values for the working-space volume measurement were

$$P_{ambient} = 1039\ cm\ H_2O\ (34.1\ ft\ H_2O)$$

$$\Delta P = 32.64\ cm\ H_2O\ (12.85\ in.\ H_2O)$$

$$V_{burrette-initial} = 17.55\ cm^3\ (1.07\ in.^3)$$

$$V_{burrette-final} = 9.25\ cm^3\ (0.564\ in.^3)$$

$$V_{connecting\ tubing} = 21.17\ cm^3\ (1.292\ in.^3)$$

$$V_{unknown} = 234\ cm^3\ (14.28\ in.^3)$$

Several readings were taken for each measurement and then averaged to arrive at the final value.

Working space	Buffer space
236.1 cm^3 (14.41 $in.^3$)	512.1 cm^3 (31.25 $in.^3$)
233.0 cm^3 (14.22 $in.^3$)	520.8 cm^3 (31.78 $in.^3$)
234.0 cm^3 (14.28 $in.^3$)	528.0 cm^3 (32.22 $in.^3$)
	522.3 cm^3 (31.87 $in.^3$)
	520.6 cm^3 (31.77 $in.^3$)
234.3 cm^3 (14.30 $in.^3$) average	520.8 cm^3 (31.78 $in.^3$) average

The volumes calculated from dimensional measurements and given in table II include an increase in the working-space volume of about 2.46 cubic centimeters (0.15 $in.^3$) because of a minor engine modification that was made after the volume measurements were completed. Thus, a "corrected" measured value of (234.3 + 2.46) = 236.8 cubic centimeters (14.45 $in.^3$) for the minimum total working-space volume should be compared with the 232.4 cubic centimeters (14.18 $in.^3$) shown in table II. There is a difference of about 2 percent between the measured and calculated values.

APPENDIX C

GPU 3 STEADY-STATE FLOW TESTS

Steady-state flow tests were made on the coolers, the regenerators, the cooler-regenerator cartridges, and the entire heater head to determine the pressure-drop-versus-mass-flow-rate characteristics. Tests were run with air at mass flow rates that gave approximately the same Reynolds numbers as actually occur in the engine. These Reynolds numbers were determined from the NASA Lewis computer simulation described in reference 1. The inlet air temperature for these tests was about 27° C (80° F). For each component, measurements were made for flow in both directions.

Flow tests were run both before and after the engine tests discussed in this report. Figures 17 to 20 give data taken before the test runs (new cooler-regenerator cartridges). Figures 17 and 18 show pressure drop versus mass flow rate for the coolers and regenerators, respectively. A range of data is shown in each figure that represents test results for 22 coolers and 16 regenerators.

Results for the assembled cooler-regenerator cartridges are given in figures 19 and 20. Figure 19 shows a range of pressure drop versus mass flow rate for the nine cartridges that were tested. Measurements for reverse flow and forward flow for one cartridge are shown in figure 20. Forward flow is defined as flow from the cooler to the regenerator.

Flow tests were made on the heater head (complete heat-exchanger circuit) and on three individual cartridges after the engine tests were finished. The cartridges had accumulated 80 hours of run time. Figure 21 gives pressure drop versus mass flow rate for the heater head for flow in both directions. It also shows the range of pressure drop for the three cartridges. The difference between the two represents the losses in the heater tubes and the losses due to entrance and exit effects for the various heat exchangers. For the heater head, the abscissa corresponds to the flow rate through just one of the cooler-regenerator paths. This was determined by dividing the total airflow through the heater head by 8. The fixture used to flow test the heater head is shown with the heater head in figure 22.

Finally, pressure drop for the cooler-regenerator cartridges when they were new is compared with that obtained after 80 hours of run time in figure 23. The figure indicates that by the conclusion of the engine tests the pressure drop had increased by about one-third from what it had been for the new cartridges.

Also, the spread of pressure drop for the three cartridges had increased. To make this plot, the data for the new cartridges were corrected from 150-psi inlet pressure to 115 psi to allow comparison to the 80-hour data.

The primary reason for the increased pressure drop was apparently oil contamination of the regenerators. Figure 24 shows the three cooler-regenerator cartridges that were removed from the heater head after the engine tests. Oil deposits found on the outside of the regenerator cans indicate that oil was migrating into the working fluid. Also, rust was present in the working fluid, as indicated by rust deposits on the cooler-end-caps at the exits of the cooler tubes. The power piston was coated with rust.

APPENDIX D

GPU 3 INSTRUMENTATION

All measurements made in this series of engine tests are described in table III. Included for each are item number, mnemonic, parameter description, instrument type, and range. The ranges listed are the full-scale instrument range for pressure gages, pressure transducers, and flowmeters and the measurement range for thermocouples. All instruments read out in U.S. customary units. In the data reduction program, data are printed out in both U.S. customary and S.I. units.

Thermocouple locations on the preheater, the cylinder, and the regenerator housings, respectively, are shown in figures 25 to 27. For dimensions needed for conduction calculations associated with these temperature measurements, see figure 16. Figure 28 gives the heater-tube metal and heater-tube gas thermocouple locations. A detailed schematic of the engine assembly is given in reference 4. Finally, figure 2 is a schematic of the test setup and shows the instrumentation locations in the facility support systems. All measurements are referenced by item number and also, with the exception of figure 2, by mnemonic.

Several instrumentation locations do not show in these figures, including those for the insulation cover temperatures and the compression-space gas temperature. The dimensions necessary for calculating conduction losses through the insulation covers are given in table I. The compression-space gas temperature is measured in the connecting passage between the cooler (cartridge 3) and the cylinder.

APPENDIX E

GPU 3 CALCULATIONS AND DATA REDUCTION PROGRAM

GPU 3 CALCULATIONS

This appendix contains a partial listing of the data reduction program used to obtain calculated quantities from the test data input. Table IV defines all calculation parameters that are printed out as part of the final data output. All calculations were done in U.S. customary units and then printed out in both U.S. customary and SI units. Table III previously defined the input data to the program. Finally, table V describes the constants used in the data reduction. The conversions to SI units and the write statements for both sets of units are not shown in the program listing.

In addition to the information in the tables, several points sould be clarified concerning the data reduction program. For zero power out of the alternator, the required engine output to overcome alternator losses at various speeds was determined during alternator calibration. That part of the program from the statement preceding statement 21 through statement 33 defines this engine output. Also, the following intermediate quantities were calculated from equations linearized over the listed temperature range:

RHO1: cooling-water density, lbm/ft^3 (50^o to 100^o F)

RHO2: oil density, lbm/ft^3 (80^o to 160^o F)

CP2: specific heat of oil, $Btu/lbm \cdot {}^oR$ (80^o to 160^o F)

CONVY: $g\beta\rho^2/\mu^2$, parameter for convection heat loss calculation, $1/ft^3 \cdot {}^oF$ (100^o to 200^o F and 200^o to 300^o F)

where $g\beta\rho^2/\mu^2$ is part of the Grashof number

CONVK: thermal conductivity of air, $Btu/hr \cdot ft \cdot {}^oR$ (100^o to 300^o F)

GASK: thermal conductivity of working fluid, $Btu/hr \cdot ft \cdot {}^oR$ (200^o to 800^o F)

SSK: thermal conductivity of stainless steel, $Btu/hr \cdot ft \cdot {}^oR$ (200^o to 600^o F and 600^o to 1200^o F)

Finally, the equations under the comment card "Calculation Change Due to Missing Data" are used to correct for a regenerator housing temperature sensor, TRH2M, that failed during the tests and thus affected the conduction calculations.

GPU 3 DATA REDUCTION PROGRAM

```
1*          DIMENSION RUNID(2)
2*         1 REAL LHV,NAFLO,MEANCP,MEANBP
3*          REAL IMEPT,INDWT,IPWR,INDEFF
4*          REAL LSHUT
5*          READ(5,2,END=1000)
6*         2 FORMAT(2X,'XXXX
```

```
58*           CLEAR=0.01
59*           ' HUT=1.525
60*     C OVE ALL QUANTITIES
61*
62*
63*           PWRIN=FFLO*LHV/2543.4
64*           PWRALT=VOLT*AMP/746.
65*           IF(PWRALT)21,22,21
66*        21 PWROUT=PWRALT/(ALTEFF+.0001)*100.
67*           GO TO 31
68*        22 IF(RPM-3250)23,24,24
69*        24 PWROUT=.35
70*           GO TO 31
71*        23 IF(RPM-2750)25,26,26
72*        26 PWROUT=.27
73*           GO TO 31
74*        25 IF(RPM-2250)27,28,28
75*        28 PWROUT=.20
76*           GO TO 31
77*        27 IF(RPM-1750)29,32,32
78*        32 PWROUT=.17
79*           GO TO 31
80*        29  IF(RPM-1250)33,34,34
81*        34 PWROUT=.11
82*           GO TO 31
83*        33 PWROUT=.07
84*        31 BRKEFF=PWROUT/PWRIN*100.
85*           RHO1=(TCWIN+459.67)*-.0077+66.34
86*           QCWCO=CWFLOC*RHO1*CP1*TDLWC/317.08
87*           BMEP=PWROUT*33000./RPM*12./VT
88*        10 BSFC=FFLO/PWROUT
89*        15 TRATIO=(TGCOMP+459.67)/(TGEXP+459.67)
90*           AFRAT=(CAFLO*60.+NAFLO)/FFLO
91*
92*
93*
94*     C HEAT BALANCE
95*           QIN=PWRIN*33000./RPM
96*           BRKOUT=PWROUT*33000./RPM
97*           RHO2=(TOILIN+459.67)*-.03463+75.44
98*           CP2=(2.*(TOILIN+459.67)+TDELO)/2.*.0004677+.1953
99*           QOILC=OILFLO*RHO2*CP2*TDELO*104./RPM
100*          TAEXHO=(TEXHO1+TEXHO2+TEXHO3)/3.
101*          QEXHC=((FFLO+NAFLO)/60.+CAFLO)*778.*CP3*(TAEXHO-TAINPM)/RPM
102*          QCWTOC=CWFLOT*RHO1*CP1*TDLWT*104./RPM
103*          QCWCOC=QCWCO*33000./RPM
104*          QCWBC=CWFLOB*RHO1*CP1*TDLWB*104./RPM
105*          QCWFVC=CWFLFV*RHO1*CP1*TDWFV*104./RPM
106*          TAPREH=(TPHOT1+TPHOT2+TPHOT3+TPHOB1+TPHOB2+TPHOB3)/6.
107*          QRADC=6.9758E-08*D1*H1*VF*(EMM*(TAPREH+459.67)**4-EMM*(TAMB+459.67
108*         1)**4)/RPM
109*          TACONV=(TAPREH+TAMB)/2.
110*          IF(TACONV-200)99,99,98
111*       98 CONVV=((TAPREH+TAMB+2.*459.67)/2.*-.00406+3.53)*1.E06
112*          GO TO 97
113*       99 CONVV=((TAPREH+TAMB+2.*459.67)/2.*-.0091+6.85)*1.E06
114*       97 CONVK=(TAPREH+TAMB+2.*459.67)/2.*2.E-05+4.207E-03
115*          CONVH=CONVK*.555/H1*(PR*H1**3*CONVV*(TAPREH-TAMB))**.25
116*          QCONVC=CONVH*A4*12.971*(TAPREH-TAMB)/RPM
```

REPRODUCIBILITY OF THE
ORIGINAL PAGE IS POOR

REPRODUCIBILITY OF THE
ORIGINAL PAGE IS POOR

```
117*            QUNACC=QIN-QCHCOC-QCWRC-QCWFVC-WRKOUT-QOILC-QEXHC-QRADC-QCONVC
118*      C CONDUCTION LOSSES
119*            T1=(TRH1T+TRH2M)/2.
120*            CALL CONDK(T1,SSK1)
121*            QRH1=A1/CL1*SSK1*(TRH1T-TRH2M)
122*            T2=(TRH2M+TRH3B)/2.
123*            CALL CONDK(T2,SSK2)
124*            QRH2=6.28318*SSK2*RI1*(R1-R0)*(TRH2M-TRH3B)/144./CL2/ALOG
125*           1((R1-RI1)*(R0+RI1)/(R1+RI1)/(R0-RI1))
126*            T3=(TRH8TI+TRH9MI)/2.
127*            CALL CONDK(T3,SSK3)
128*            QRH3=A1/CL1*SSK3*(TRH8TI-TRH9MI)
129*            T4=(TRH9MI+TRH10B)/2.
130*            CALL CONDK(T4,SSK4)
131*            QRH4=6.28318*SSK4*RI1*(R1-R0)*(TRH9MI-TRH10B)/144./CL2/ALOG
132*           1((R1-RI1)*(R0+RI1)/(R1+RI1)/(R0-RI1))
133*            T5=(TCYL3+TCYL4)/2.
134*            CALL CONDK(T5,SSK5)
135*            QCYL1=6.28318*SSK5*RI2*(R3-R2)*(TCYL3-TCYL4)/144./CL3/ALOG
136*           1((R3-RI2)*(R2+RI2)/(R3+RI2)/(R2-RI2))
137*            T6=(TCYL4+TCYL5B)/2.
138*            CALL CONDK(T6,SSK6)
139*            QCYL2=6.28318*SSK6*RI2*(R4-R3)*(TCYL4-TCYL5B)/144./CL4/ALOG
140*           1((R4-RI2)*(R3+RI2)/(R4+RI2)/(R3-RI2))
141*            T7=(TIC1T+TIC2B)/2.
142*            CALL CONDK(T7,SSK7)
143*            QINSC=A3/CL6*SSK7*(TIC1T-TIC2B)
144*            T8=(TGCOMP+TGEXP)/2.
145*            CALL CONDK(T8,SSK8)
146*            QDISP=A2/CL5*SSK8*(TGEXP-TGCOMP)
147*      C     THERMAL CONDUCTIVITY OF WORKING FLUID;HELIUM:0,HYDROGEN:1
148*            IF(GMARK)82,81,82
149*        81  GASK=6.850E-05*(TCYL3+459.67+TCYL5B+459.67)/2.+0.05401
150*            GO TO 83
151*        82  GASK=1.063E-04*(TCYL3+459.67+TCYL5B+459.67)/2.+0.05421
152*        83  QSHUT=GASK*3.14159*QSHUT*STROKE**2*(TCYL3-TCYL5B)/(8.*CLEAR
153*           1*LSHUT*12.)
154*            QCONDT=(QRH1+QRH3)*8./2.+QCYL1+QSHUT+QINSC+QDISP
155*            QING=PWRIN*2545.-(QRADC+QCONVC+QEXHC+QCWFVC)*RPM*.077-(QRH1+QRH3)
156*           1*8./2.-QCYL1-QDISP-QINSC-QSHUT
157*            QOUT=QCWCO*2545.-QCYL1-(QRH1+QRH3)*8./2.-QDISP-QINSC-QSHUT
158*            QINEH=QING+QCONDT
159*            QINEC=(WRKOUT+QOILC+QCWBC+QCWCOC)*RPM*.077
160*      C CALCULATION CHANGE DUE TO MISSING DATA
161*            IF(DMARK)17,18,17
162*         17 QRH1=0.0
163*            QRH2=0.0
164*            QCONDT=QRH3*8.+QCYL1+QSHUT+QINSC+QDISP
165*            QING=PWRIN*2545.-(QRADC+QCONVC+QEXHC+QCWFVC)*RPM*.077-QRH3
166*           1*8.    -QCYL1-QDISP-QINSC-QSHUT
167*            QOUT=QCWCO*2545.-QCYL1-QRH3*8.          -QDISP-QINSC-QSHUT
168*            QINEH=QING+QCONDT

  1*            SUBROUTINE CONDK(Z,SSK)
  2*            IF(Z-600.)20,20,30
  3*         20 SSK=.00387*Z+8.571
  4*         30 SSK=.00476*Z+7.977
  5*            RETURN
  6*            END
```

APPENDIX F

GPU 3 MICROFICHED DATA AND SAMPLE DATA POINT

A complete listing of the detailed test data for the 67 data points taken during this series of engine tests is included on microfiche in the back of this report. The printout for each data point includes the test data, as well as the results of all calculations computed from the test data. These are shown in both U.S. customary and SI units. As an example of what is available on microfiche, this appendix contains a listing for a sample data point. The information needed to understand the computer listings is contained in this appendix and in appendixes D and E. The mnemonics for the test data are explained in table III and those for the calculations in table IV.

Each data point is identified by run number, date, and time of the data scan. The run number consists of five alphanumeric characters and is explained as follows, where the sample data point (run number HE3-63B) is used as an example:

(a) HE helium working fluid
H hydrogen working fluid

REPRODUCIBILITY OF THE ORIGINAL PAGE IS POOR

(b) 3 1300° F heater-tube gas temperature
2 1200° F heater-tube gas temperature
1 1100° F heater-tube gas temperature

(c) 10 1000-psi mean compression-space pressure
8 800-psi mean compression-space pressure
6 600-psi mean compression-space pressure
4 400-psi mean compression-space pressure
2 200-psi mean compression-space pressure

(d) 1 3500-rpm engine speed
2 3000-rpm engine speed
3 2500-rpm engine speed
4 2000-rpm engine speed
5 1500-rpm engine speed
6 1000-rpm engine speed
R reference point - initial point established after each engine startup - heater-tube gas temperature, 1300° F; engine speed, 3000 rpm; no load

(e) A first data scan

B second data scan

Therefore, HE3-63B indicates helium working fluid, 1300° F heater-tube gas temperature, 600-psi mean compression-space pressure, 2500-rpm engine speed, and second data scan.

Several measurements (primarily temperatures) were not recorded for parts of the tests because of malfunctioning instrumentation. These measurements are indicated by a zero under the appropriate mnemonic.

As a final comment, it appears from an analysis of the data that most errors in the energy balance (QUNACC) were due to inaccuracies in the exhaust loss measurement or in the radiation and convection loss calculation.

A listing for a sample data point follows.

RUN NUMBER: HE3-630 DATE: 6/6/78 REAL TIME: 2:54

U.S. CUSTOMARY UNITS

STEADY STATE TEST DATA

RUNTIM (HR)	TAMB (F)	TGDUM2 (F)	TALTH (F)	TFINN (F)	TAINN (F)	TAINPH (F)	TOILIN (F)	TCWIN (F)
135.5	92.	1313.	163.	82.	87.	83.	148.	54.

TDELO (F)	TDLWT (F)	TDLWC (F)	TDLWB (F)	TDWFV (F)	TGBUF (F)	TGCOMP (F)	TGEXP (F)	TGDUM1 (F)	TEXHO1 (F)
4.4	18.3	18.5	16.1	4.3	124.	708.	1259.	1267.	479.

TEXHO2 (F)	TEXHO3 (F)	TPHOT1 (F)	TPHOT2 (F)	TPHOT3 (F)	TPHOB1 (F)	TPHOB2 (F)	TPHOB3 (F)	TPHIT1 (F)
859.	803.	466.	791.	718.	185.	362.	224.	923.

TPHIT2 (F)	TPHIT3 (F)	TPHIB1 (F)	TPHIB2 (F)	TPHIB3 (F)	TRH1T (F)	TRH2M (F)	TRH3B (F)	TRH4C (F)	TRH5C (F)
1166.	1014.	867.	1053.	780.	1056.	812.	372.	791.	814.

TRH6C (F)	TRH7C (F)	TRH8TI (F)	TRH9MI (F)	TRH10B (F)	TCYL1T (F)	TCYL2 (F)	TCYL3 (F)	TCYL4 (F)	TCYL5B (F)
741.	806.	1061.	798.	293.	1300.	1194.	1076.	721.	527.

TCYL6C (F)	TCYL7C (F)	TCYL8C (F)	TIC1T (F)	TIC2B (F)	THT1DT (F)	THT2DM (F)	THT3DB (F)	THT4RT (F)	THT5RB (F)
1059.	1035.	1118.	795.	584.	1469.	1479.	1487.	0.	1354.

THT6C (F)	THT7C (F)	THT8C (F)	THT9T (F)	THT10B (F)	THT11E (F)	THT12R (F)	MEANCP (PSI)	MEANBP (PSI)
1385.	1396.	1475.	1529.	1373.	1218.	1157.	600.	692.

AMP (AMPS)	VOLT (VOLTS)	RPM (RPM)	CWFLOT (GPM)	CWFLOC (GPM)	CWFLOB (GPM)	CWFLFV (GPM)	OILFLO (GPM)
68.3	31.5	2503.	3.87	3.05	.43	.49	.51

FFLO (LB/HR)	CAFLO (LB/MIN)	NAFLO (LB/HR)	POIL (PSI)	PFNOZ (PSIL	PCOAIR (IN H2O)	PNOAIR (PSI)	RLOAD (AMPS)
3.827	2.73	1.51	56.	9.7	15.5	1.1	62.

TGDUM3 (F)
1280.

REPRODUCIBILITY OF THE
ORIGINAL PAGE IS POOR

DYNAMIC TEST DATA

PDCOMP (PSI)	PDEXP (PSI)	PDBUF (PSI)	AMINCP (DEG)	AMAXCP (DEG)	AMINEP (DEG)	AMAXEP (DEG)	AMINBP (DEG)	AMAXBP (DEG)
426.	420.	273.	285.	70.	295.	70.	55.	255.

STEADY STATE CALCULATIONS

OVERALL QUANTITIES

PWRIN (HP)	PWRALT (HP)	PWROUT (HP)	ALTEFF (%)	BRKEFF (%)	QCWCO (HP)
27.96	2.884	3.552	81.2	12.70	11.10

BMEP (PSI)	BSFC (LB/HP-HR)	TRATIO (DIMEN)	AFRAT (DIMEN)
77.03	1.078	.388	43.2

HEAT BALANCE

QIN (FT-LB)	WRKOUT (FT-LB)	QOILC (FT-LB)	TAEXHO (F)	QEXHC (FT-LB)	QCWTOC (FT-LB)	QCWCOC (FT-LB)
368.67	46.83	2.44	713.7	138.15	183.57	146.36

QCWBC (FT-LB)	QCWFVC (FT-LB)	TAPREH (F)	QRADC (FT-LB)	CONVH (BTU/HR-SQ FT-F)	QCONVC (FT-LB)	QUNACC (FT-LB)
17.95	5.46	457.7	4.73	1.282	4.21	2.55

CONDUCTION LOSSES

QRH1 (BTU/HR)	QRH2 (BTU/HR)	QRH3 (BTU/HR)	QRH4 (BTU/HR)	QCYL1 (BTU/HR)	QCYL2 (BTU/HR)	QSHUT (BTU/HR)
128.3	134.5	138.1	151.2	626.4	669.6	698.3

QINSC (BTU/HR)	QDISP (BTU/HR)	QCONDT (BTU/HR)	QING (BTU/HR)	QOUT (BTU/HR)	QINEH (BTU/HR)	QINEC (BTU/HR)
395.9	307.7	3094.	38670.	25159.	41764.	41162.

S.I. UNITS

STEADY STATE TEST DATA

RUNTIM (HR)	TAMB (C)	TGDUM2 (C)	TALTH (C)	TFINN (C)	TAINN (C)	TAINPH (C)	TOILIN (C)	TCWIN (C)
135.5	33.	712.	73.	28.	31.	28.	64.	12.

TDELO (C)	TDLWT (C)	TDLWC (C)	TDLWB (C)	TDWFV (C)	TGBUF (C)	TGCOMP (C)	TGEXP (C)	TGDUM1 (C)	TEXHO1 (C)
2.4	10.2	10.3	8.9	2.4	51.	98.	682.	686.	248.

TEXHO2 (C)	TEXHO3 (C)	TPHOT1 (C)	TPHOT2 (C)	TPHOT3 (C)	TPHOB1 (C)	TPHOB2 (C)	TPHOB3 (C)	TPHIT1 (C)
459.	428.	241.	422.	381.	85.	183.	107.	495.

TPHIT2 (C)	TPHIT3 (C)	TPHIB1 (C)	TPHIB2 (C)	TPHIB3 (C)	TRH1T (C)	TRH2M (C)	TRH3B (C)	TRH4C (C)	TRH5C (C)
630.	546.	464.	567.	416.	569.	433.	189.	422.	434.

TRH6C (C)	TRH7C (C)	TRH8TI (C)	TRH9MI (C)	TRH10B (C)	TCYL1T (C)	TCYL2 (C)	TCYL3 (C)	TCYL4 (C)	TCYL5B (C)
394.	430.	572.	426.	145.	704.	646.	580.	383.	275.

TCYL6C (C)	TCYL7C (C)	TCYL8C (C)	TIC1T (C)	TIC2B (C)	THT1DT (C)	THT2DM (C)	THT3DB (C)	THT4RT (C)	THT5RB (C)
571.	557.	603.	424.	307.	798.	804.	808.	0.	734.

THT6C (C)	THT7C (C)	THT8C (C)	THT9T (C)	THT10B (C)	THT11E (C)	THT12R (C)	MEANCP (MPA)	MEANBP (MPA)
752.	758.	802.	832.	745.	659.	625.	4.13	4.77

AMP (AMPS)	VOLT (VOLTS)	RPM (RPM)	CWFLOT (LPM)	CWFLOC (LPM)	CWFLOB (LPM)	CWFLFV (LPM)	OILFLO (LPM)
68.3	31.5	2503.	14.6	11.5	1.63	1.85	1.93

FFLO (G/HR)	CAFLO (G/MIN)	NAFLO (G/HR)	POIL (KPA)	PFNOZ (KPA)	PCOAIR (KPA)	PNOAIR (KPA)	RLOAD (AMPS)
1736.	1238.	685.	386.	66.9	3.85	7.58	62.

TGDUM3 (C)
693.

REPRODUCIBILITY OF THE ORIGINAL PAGE IS POOR

DYNAMIC TEST DATA

PDCOMP (MPA)	PDEXP (MPA)	PDBUF (MPA)	AMINCP (DEG)	AMAXCP (DEG.)	AMINEP (DEG)	AMAXEP (DEG)	AMINBP (DEG)	AMAXBP (DEG)
2.94	2.89	1.88	285.	70.	295.	70.	55.	255.

STEADY STATE CALCULATIONS

OVERALL QUANTITIES

PWRIN (KW)	PWRALT (KW)	PWROUT (KW)	ALTEFF (%)	BRKEFF (%)	QCWCO (KW)
20.85	2.151	2.649	81.2	12.70	8.28

BMEP (MPA)	BSFC (G/KW-HR)	TRATIO (DIMEN)	AFRAT (DIMEN)
531.1	655.	.388	43.2

HEAT BALANCE

QIN (JOULES)	WRKOUT (JOULES)	QOILC (JOULES)	TAEXHO (C)	QEXHC (JOULES)	QCWTOC (JOULES)	QCWCOC (JOULES)
499.55	63.45	3.30	379.	187.19	248.74	198.32

QCWBC (JOULES)	QCWFVC (JOULES)	TAPREH (C)	QRADC (JOULES)	CONVH (WATTS-SQ M-C)	QCONVC (JOULES)	QUNACC (JOULES)
24.32	7.40	236.	6.41	2.2488	5.70	3.45

CONDUCTION LOSSES

QRH1 (WATTS)	QRH2 (WATTS)	QRH3 (WATTS)	QRH4 (WATTS)	QCYL1 (WATTS)	QCYL2 (WATTS)	QSHUT (WATTS)
37.6	39.4	40.5	44.3	183.5	196.1	204.5

QINSC (WATTS)	QDISP (WATTS)	QCONDT (WATTS)	QING (WATTS)	QOUT (WATTS)	QINFH (WATTS)	QINEC (WATTS)
116.0	90.1	906.	11327.	7369.	12233.	12057.

REFERENCES

1. Tew, Roy; Jeffries, Kent; and Miao, David: A Stirling Engine Computer Model for Performance Calculations. DOE/NASA/1011-78/24, NASA TM-78884, 1978.

2. Tew, Roy C., Jr.; Thieme, Lanny G.; and Miao, David: Initial Comparison of Single-Cylinder Stirling Engine Computer Model Predictions with Test Results. DOE/NASA/1040-78/30, NASA TM-79044, 1979.

3. Thieme, Lanny G.; and Tew, Roy C., Jr.: Baseline Performance of the GPU 3 Stirling Engine. DOE/NASA/1040-78/5, NASA TM-79038, 1978.

4. Cairelli, J. E.; Thieme, L. G.; and Walter, R. J.: Initial Test Results with a Single-Cylinder Rhombic-Drive Stirling Engine. DOE/NASA/1040-78/1, NASA TM-78919, 1978.

5. Rice, William J.: Indicated Mean Effective Pressure Instrument. NASA Tech Brief B76-10542, 1977.

6. A Collection of Stirling Engine Reports from General Motors Research 1958 - 1970, Part 6: Regenerators. GMR-2690, Pt. 6, General Motors Research Labs., 1978.

7. Potential Capabilities of the Stirling Engine for Space Power. EDR-3097, General Motors Corp., 1963. (ASD-TDR-62-1099, AD-403698.)

TABLE I. - GPU 3 ENGINE DIMENSIONS AND PARAMETERS

Number of cylinders	1
Type of engine	Displacer
Type of drive	Rhombic
Type of shaft seals	Sliding
Miscellaneous:	
Cylinder bore with liner, cm (in.)	6.99 (2.75)
Cylinder bore above liner (top of displacer seal at top of liner at displacer top-dead-center), cm (in.)	7.01 (2.76)
Stroke, cm (in.)	3.15 (1.24)
Displacement (maximum change in total working-space volume), cm^3 ($in.^3$)	119.6 (7.30)
Piston-rod diameter, cm (in.)	2.22 (0.875)
Displacer-rod diameter, cm (in.)	0.953 (0.375)
Displacer diameter, cm (in.)	6.96 (2.74)
Displacer wall thickness, cm (in.)	0.159 (0.0625)
Expansion-space clearance, cm (in.)	0.163 (0.064)
Compression-space clearance, cm (in.)	0.030 (0.012)
Cooler:	
Tube length, cm (in.)	4.60 (1.81)
Heat-transfer length, cm (in.)	3.56 (1.40)
Tube inside diameter, cm (in.)	0.108 (0.0425)
Tube outside diameter, cm (in.)	0.159 (0.0625)
Number of tubes per cylinder	312
Number of tubes per cooler	39
Heater:	
Mean tube length, cm (in.)	
Regenerator side	12.90 (5.08)
Cylinder side	11.63 (4.58)
Heat-transfer length, cm (in.)	7.77 (3.06)
Tube inside diameter, cm (in.)	0.302 (0.119)
Tube outside diameter, cm (in.)	0.483 (0.190)
Number of tubes per cylinder (consider tubes to regenerator and cylinder separately)	80
Regenerators:	
Length (inside), cm (in.)	2.26 (0.89)
Diameter (inside), cm (in.)	2.26 (0.89)
Number per cylinder	8
Matrix:	
Wire-cloth material	304 stainless steel
Cloth mesh per 2.5 cm (1 in.)	200×200
Wire diameter, cm (in.)	0.00406 (0.0016)
Number of layers	308
Filler factor, percent	30.3
Drive:	
Connecting-rod length, cm (in.)	4.60 (1.81)
Crank radius, cm (in.)	1.38 (0.543)
Eccentricity, cm (in.)	2.08 (0.82)
Insulation covers:	
Cross-sectional area, cm^2 ($in.^2$)	6.45 (1.00)
Length between thermocouples, cm (in.)	1.27 (0.50)

REPRODUCIBILITY OF THE
ORIGINAL PAGE IS POOR

TABLE II. - GPU 3 ENGINE DEAD VOLUMES

[All volumes in cm^3 ($in.^3$).]

Expansion space clearance volume:		
Clearance around displacer	3.34	(0.204)
Clearance above displacer	7.41	(0.452)
Volume from end of heater tubes into cylinder	1.74	(0.106)
Total	12.49	(0.762)
Heater dead volume:		
Insulated portion of tubes leading to expansion space	9.68	(0.591)
Heated portion of tubes	47.46	(2.896)
Insulated portion of tubes leading to regenerator	13.29	(0.811)
Additional volume in four tubes used for instrumentation	2.74	(0.167)
Volume in header	7.67	(0.468)
Total	80.84	(4.933)
Regenerator dead volume:		
Volume between regenerators and heater tubes	8.75	(0.534)
Volume within matrix	50.60	(3.088)
Volume between regenerators and cooler tubes	6.16	(0.376)
Total	65.51	(3.998)
Cooler dead volume:		
Volume in cooler tubes	13.14	(0.802)
Compression-space clearance volume:		
Volume in connecting passages from cooler tubes to compression space	12.57	(0.767)
Clearance around power piston	7.36	(0.449)
Clearance between displacer and power piston	1.26	(0.077)
Total	21.19	(1.293)
Total dead volume:	193.2	(11.79)
Minimum live volume (power piston at TDC)	39.2	(2.39)
Calculated minimum total working-space volume	232.4	(14.18)

TABLE III. - GPU 3 INSTRUMENTATION

[All thermocouples are Chromel-Alumel (type K); thermopiles are Chromel-constantan. Listed ranges are full-scale range for pressure transducers, pressure gages, and flowmeters and measurement range for thermocouples. Pressure phase angles are determined by using a marker channel generated from the crankshaft angle signal (crankshaft angle measured with shaft encoder).]

Item	Mnemonic	Parameter	Instrument	Range
1	RUNTIM	Accumulative engine run-time	----------	----------
2	TAMB	Ambient air temperature	Liquid-in-glass thermometer	50^{o} - 100^{o} F
3	TALTH	Alternator housing temperature	Thermocouple	60^{o} - 250^{o} F
4	TFINN	Fuel inlet temperature		60^{o} - 100^{o} F
5	TAINN	Air inlet temperature - nozzle		60^{o} - 100^{o} F
6	TAINPH	Air inlet temperature - preheater		60^{o} - 100^{o} F
7	TOILIN	Engine oil inlet temperature		80^{o} - 200^{o} F
8	TCWIN	Cooling-water inlet temperature		50^{o} - 70^{o} F
9	TDELO	Engine oil delta temperature - outlet to inlet	Thermopile	1^{o} - 10^{o} F
10	TDLWT	Cooling-water delta temperature - total flow out to in		3^{o} - 35^{o} F
11	TDLWC	Cooling-water delta temperature - cooler outlet to inlet		3^{o} - 35^{o} F
12	TDLWB	Cooling-water delta temperature - buffer outlet to inlet		3^{o} - 35^{o} F
13	TDWFV	Cooling-water delta temperature - nozzle outlet to inlet		1^{o} - 10^{o} F
14	TGDUM1	Heater-tube gas temperature - instrumentation tube 1	Thermocouple	1000^{o} - 1350^{o} F
15	TGDUM2	Heater-tube gas temperature - instrumentation tube 2		1000^{o} - 1350^{o} F
16	TGDUM3	Heater-tube gas temperature - instrumentation tube 4		1000^{o} - 1350^{o} F
17	TGBUF	Buffer-space gas temperature		70^{o} - 150^{o} F
18	TGCOMP	Compression-space gas temperature		70^{o} - 250^{o} F
19	TGEXP	Expansion-space gas temperature		1000^{o} - 1300^{o} F
20	TEXHO1	Exhaust temperature out of preheater - 0^{o}		300^{o} - 1000^{o} F
21	TEXHO2	Exhaust temperature out of preheater - 120^{o}		300^{o} - 1000^{o} F
22	TEXHO3	Exhaust temperature out of preheater - 240^{o}		300^{o} - 1000^{o} F
23	TPHOT1	Preheater outside surface temperature - top - 0^{o}		100^{o} - 900^{o} F
24	TPHOT2	Preheater outside surface temperature - top - 120^{o}		
25	TPHOT3	Preheater outside surface temperature - top - 240^{o}		
26	TPHOB1	Preheater outside surface temperature - bottom - 0^{o}		
27	TPHOB2	Preheater outside surface temperature - bottom - 120^{o}		
28	TPHOB3	Preheater outside surface temperature - bottom - 240^{o}		
29	TPHIT1	Preheater inside surface temperature - top - 0^{o}		500^{o} - 1300^{o} F
30	TPHIT2	Preheater inside surface temperature - top - 120^{o}		500^{o} - 1300^{o} F

REPRODUCIBILITY OF THE ORIGINAL PAGE IS POOR

TABLE III. - Continued.

Item	Mnemonic	Parameter	Instrument	Range
31	TPHIT3	Preheater inside surface temperature - top - 240°	Thermocouple	500° - 1300° F
32	TPHIB1	Preheater inside surface temperature - bottom - 0°		
33	TPHIB2	Preheater inside surface temperature - bottom - 120°		
34	TPHIB3	Preheater inside surface temperature - bottom - 240°		
35	THR1T	Regenerator housing temperature - outside vertical profile - top		900° - 1200° F
36	TRH2M	Regenerator housing temperature - outside vertical profile - middle		600° - 900° F
37	TRH3B	Regenerator housing temperature - outside vertical profile - bottom		200° - 500° F
38	TRH4C	Regenerator housing temperature - circumferential profile - 0°		600° - 900° F
39	TRH5C	Regenerator housing temperature - circumferential profile - 90°		
40	TRH6C	Regenerator housing temperature - circumferential profile - 180°		
41	TRH7C	Regenerator housing temperature - circumferential profile - 270°		
42	TRH8TI	Regenerator housing temperature - inside vertical profile - top		900° - 1200° F
43	TRH9MI	Regenerator housing temperature - inside vertical profile - middle		600° - 900° F
44	TRH10B	Regenerator housing temperature - inside vertical profile - bottom		200° - 500° F
45	TCYL1T	Cylinder temperature - vertical profile - top		900° - 1400° F
46	TYCL2	Cylinder temperature - vertical profile		900° - 1400° F
47	TYCL3	Cylinder temperature - vertical profile; circumferential profile - 0°		900° - 1400° F
48	TCYL4	Cylinder temperature - vertical profile		400° - 900° F
49	TCYL5B	Cylinder temperature - vertical profile - bottom		400° - 900° F
50	TCYL6C	Cylinder temperature - circumferential profile - 90°		900° - 1400° F
51	TCYL7C	Cylinder temperature - circumferential profile - 180°		900° - 1400° F
52	TCYL8C	Cylinder temperature - circumferential profile - 270°		900° - 1400° F
53	TIC1T	Insulation-cover temperature - top		400° - 800° F
54	TIC2B	Insulation-cover temperature - bottom		400° - 800° F
55	THT1DT	Heater-tube metal temperature - instrumentation tube 1 - top		1100° - 1500° F
56	THT2DM	Heater-tube metal temperature - instrumentation tube 1 - middle - 0°		
57	THT3DB	Heater-tube metal temperature - instrumentation tube 1 - bottom		
58	THT4RT	Heater-tube metal temperature - regenerator tube - top		
59	THT5RB	Heater-tube metal temperature - regenerator tube - bottom		

TABLE III. - Concluded.

Item	Mnemonic	Parameter	Instrument	Range
60	THT6C	Heater-tube metal temperature - instrumentation tube 2 - middle - 90°	Thermocouple	1100° - 1500° F
61	THT7C	Heater-tube metal temperature - instrumentation tube 3 - middle - 180°	↓	↓
62	THT8C	Heater-tube metal temperature - instrumentation tube 4 - middle - 270°		
63	THT9T	Heater-tube metal temperature - cylinder tube - top		
64	THT10B	Heater-tube metal temperature - cylinder tube - bottom		
65	THT11E	Heater-tube metal temperature - insulated portion of instrumentation tube 1		900° - 1300° F
66	THT12R	Heater-tube metal temperature - insulated portion of regenerator tube		900° - 1300° F
67	MEANCP	Mean compression-space pressure	Strain gage transducer	0 - 1000 psig
68	MEANBP	Mean buffer-space pressure	Strain gage transducer	0 - 1500 psig
69	AMP	Alternator output current	Ammeter	0 - 150 A
70	VOLT	Alternator output voltage	Voltmeter	0 - 60 V
71	RPM	Engine speed	Pulse type with frequency meter	500 - 4000 rpm
72	CWFLOT	Cooling-water flow - total	Turbine flowmeter	1 - 10 gal/min
73	CWFLOC	Cooling-water flow - cooler	↓	1 - 10 gal/min
74	CWFLOB	Cooling-water flow - buffer		0.1 - 1.25 gal/min
75	CWFLFV	Cooling-water flow - nozzle		0.1 - 1.25 gal/min
76	OILFLO	Engine oil flow		0.05 - 0.5 gal/min
77	FFLO	Fuel flow	Weight-time method	1 - 6 lb/hr
78	CAFLO	Combustion airflow	Mass flowmeter	0.4 - 4 lb/min
79	NAFLO	Nozzle airflow	Mass flowmeter	0.2 - 2 lb/hr
80	POIL	Engine oil pressure	Gage	0 - 100 psig
81	PFNOZ	Nozzle fuel pressure	↓	0 - 15 psig
82	PCOAIR	Combustion air pressure		0 - 35 in. H_2O
83	PNOAIR	Nozzle air pressure		0 - 15 psig
84	RLOAD	Resistance load bank setting	---	---
--	PDCOMP	Pressure swing (minimum to maximum) - compression space		
--	AMINCP	Angle from displacer TDC - minimum compression-space pressure	Miniature strain gage transducer	0 - 3000 psig
--	AMAXCP	Angle from displacer TDC - maximum compression-space pressure		
--	PDEXP	Pressure swing - expansion space		
--	AMINEP	Angle from displacer TDC - minimum expansion-space pressure	Miniature strain gage transducer	0 - 2000 psig
--	AMAXEP	Angle from displacer TDC - maximum expansion-space pressure		
--	PDBUF	Pressure swing - buffer space		
--	AMINBP	Angle from displacer TDC - minimum buffer-space pressure	Miniature strain gage transducer	0 - 3000 psig
--	AMAXBP	Angle from displacer TDC - maximum buffer-space pressure		

TABLE IV. - GPU 3 CALCULATIONS

Mnemonic	Calculation
Miscellaneous:	
PWRIN	Power in from fuel, hp
PWRALT	Alternator output power, hp
PWROUT	Engine output power, hp
ALTEFF	Alternator efficiency, percent
BRKEFF	Brake thermal efficiency, percent
QCWCO	Power out to cooling water - from coolers, hp
BMEP	Brake mean effective pressure, psi
BSFC	Brake specific fuel consumption, lb/hp · hr
TRATIO	Temperature ratio - compression-space gas to expansion-space gas, dimensionless
AFRAT	Air-fuel ratio, dimensionless
Heat balance:	
QIN	Heat in from fuel per cycle, ft-lb
WRKOUT	Engine output per cycle, ft-lb
QOILC	Heat out to oil per cycle, ft-lb
TAEXHO	Average exhaust temperature out of preheater, ^{o}F
QEXHC	Heat out to exhaust per cycle, ft-lb
QCWTOC	Heat out to cooling water per cycle - total flow, ft-lb
QCWCOC	Heat out to cooling water per cycle - from coolers, ft-lb
QCWBC	Heat out to cooling water per cycle - from buffer space, ft-lb
QCWFVC	Heat out to cooling water per cycle - from fuel nozzle, ft-lb
TAPREH	Average preheater outside surface temperature, ^{o}F
QRADC	Heat out to surroundings by radiation per cycle, ft-lb
CONVH	Convection heat-transfer coefficient, Btu/hr · ft^2 · ^{o}F
QCONVC	Heat out to surroundings by convection per cycle, ft-lb
QUNACC	Unaccounted heat per cycle, ft-lb
Conduction losses:	
QRH1	Heat loss by conduction through regenerator housing - station 1, Btu/hr
QRH2	Heat loss by conduction through regenerator housing - station 2, Btu/hr
QRH3	Heat loss by conduction through regenerator housing - station 3, Btu/hr
QRH4	Heat loss by conduction through regenerator housing - station 4, Btu/hr
QCYL1	Heat loss by conduction through cylinder - station 1, Btu/hr
QCYL2	Heat loss by conduction through cylinder - station 2, Btu/hr
QSHUT	Shuttle heat loss, Btu/hr
QINSC	Heat loss by conduction through insulation covers, Btu/hr
QDISP	Heat loss by conduction through displacer, Btu/hr
QCONDT	Total conduction heat losses, Btu/hr
QING	Heat into working fluid, Btu/hr
QOUT	Heat out of working fluid, Btu/hr
QINEH	Heat into engine - hot-end heat balance, Btu/hr
QINEC	Heat into engine - cold-end heat balance, Btu/hr

TABLE V. - CONSTANTS FOR GPU 3 DATA REDUCTION PROGRAM

Mnemonic	Description of constant
LHV	Lower heating value of No. 1 diesel fuel, Btu/lbm
CP1	Specific heat of cooling water, Btu/lbm · ^{o}F
CP3	Approximate specific heat of exhaust gases, Btu/lbm · ^{o}F
VSWEPT	Volume swept in expansion space, in.^{3}
VT	Maximum change in total working-space volume, in.^{3}
A1	Cross-sectional area of regenerator housing - top, ft^{2}
A2	Cross-sectional area of displacer wall, ft^{2}
A3	Cross-sectional area of insulation cover, ft^{2}
A4	Outside surface area of preheater, ft^{2}
CL1	Conduction length for regenerator housing - stations 1 and 3, ft
CL2	Conduction length for regenerator housing - stations 2 and 4, ft
CL3	Conduction length for cylinder - station 1, ft
CL4	Conduction length for cylinder - station 2, ft
CL5	Conduction length for displacer, ft
CL6	Conduction length for insulation cover, ft
RI1	Inner radius of regenerator housing, in.
RI2	Inner radius of cylinder housing, in.
R0	Outer radius of regenerator housing - middle, in.
R1	Outer radius of regenerator housing - bottom, in.
R2	Outer radius of cylinder housing - top, in.
R3	Outer radius of cylinder housing - middle, in.
R4	Outer radius of cylinder housing - bottom, in.
D1	Outside diameter of preheater, ft
H1	Outside preheater height for losses to surroundings, ft
VF	View factor for radiation losses, dimensionless
EMM	Emissivity for radiation losses, dimensionless
PR	Prandtl number for air for convection losses, dimensionless
DSHUT	Average diameter of gap between displacer and cylinder, in.
STROKE	Piston stroke, in.
CLEAR	Clearance between displacer and cylinder, in.
LSHUT	Displacer length for shuttle calculation, in.

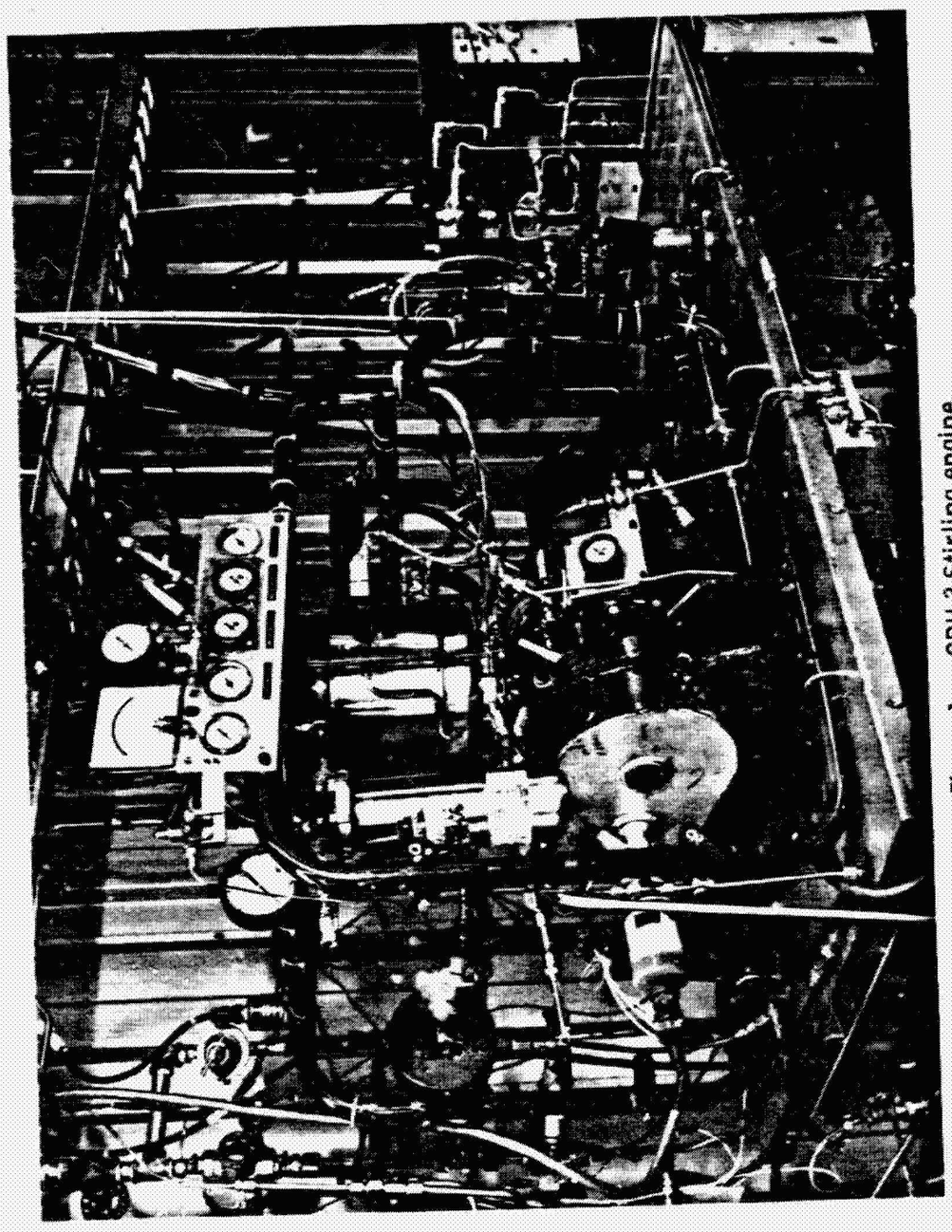

Figure 1. - GPU 3 Stirling engine.

REPRODUCIBILITY OF THE
ORIGINAL PAGE IS POOR

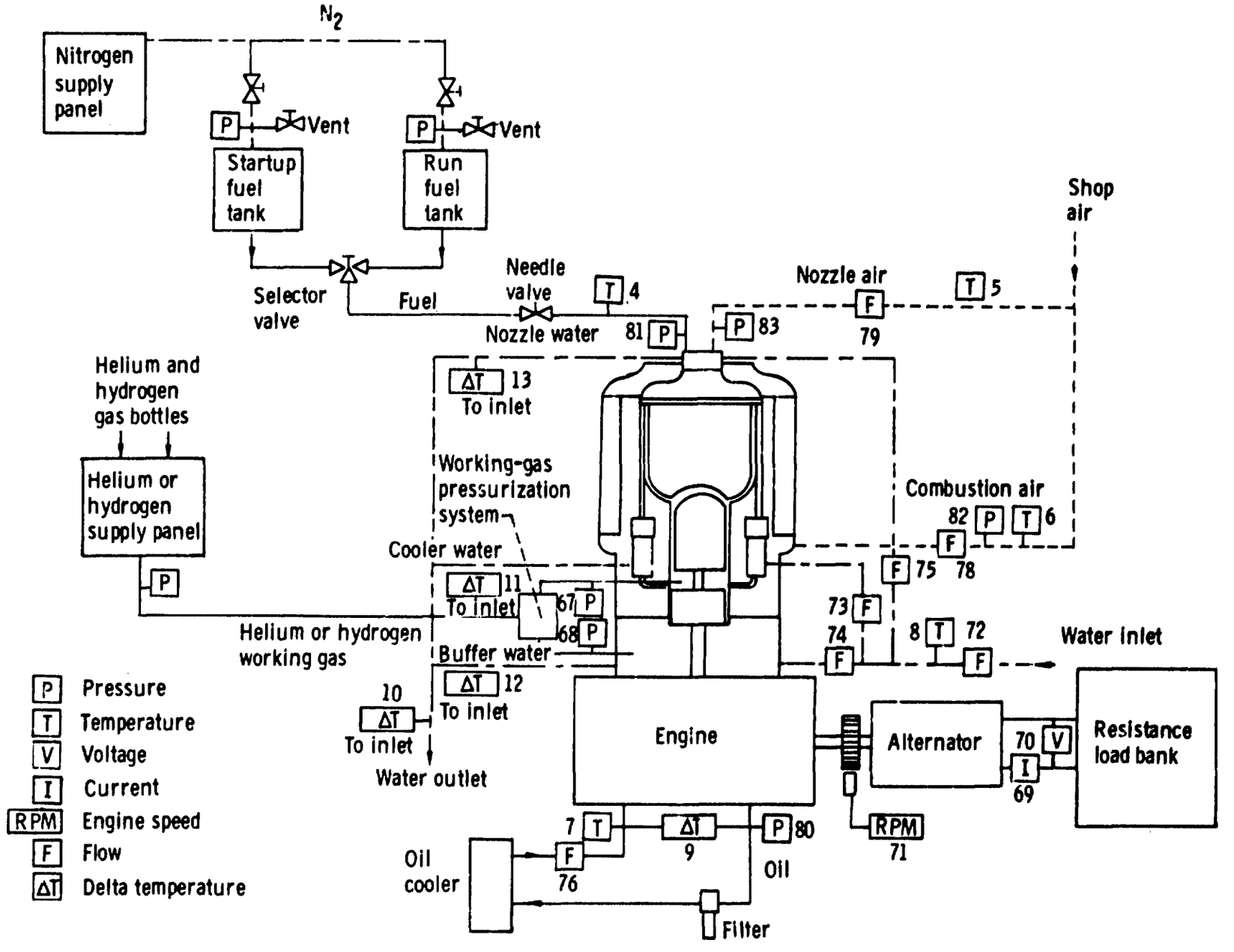

Figure 2. - GPU 3 test schematic.

REPRODUCIBILITY OF THE
ORIGINAL PAGE IS POOR

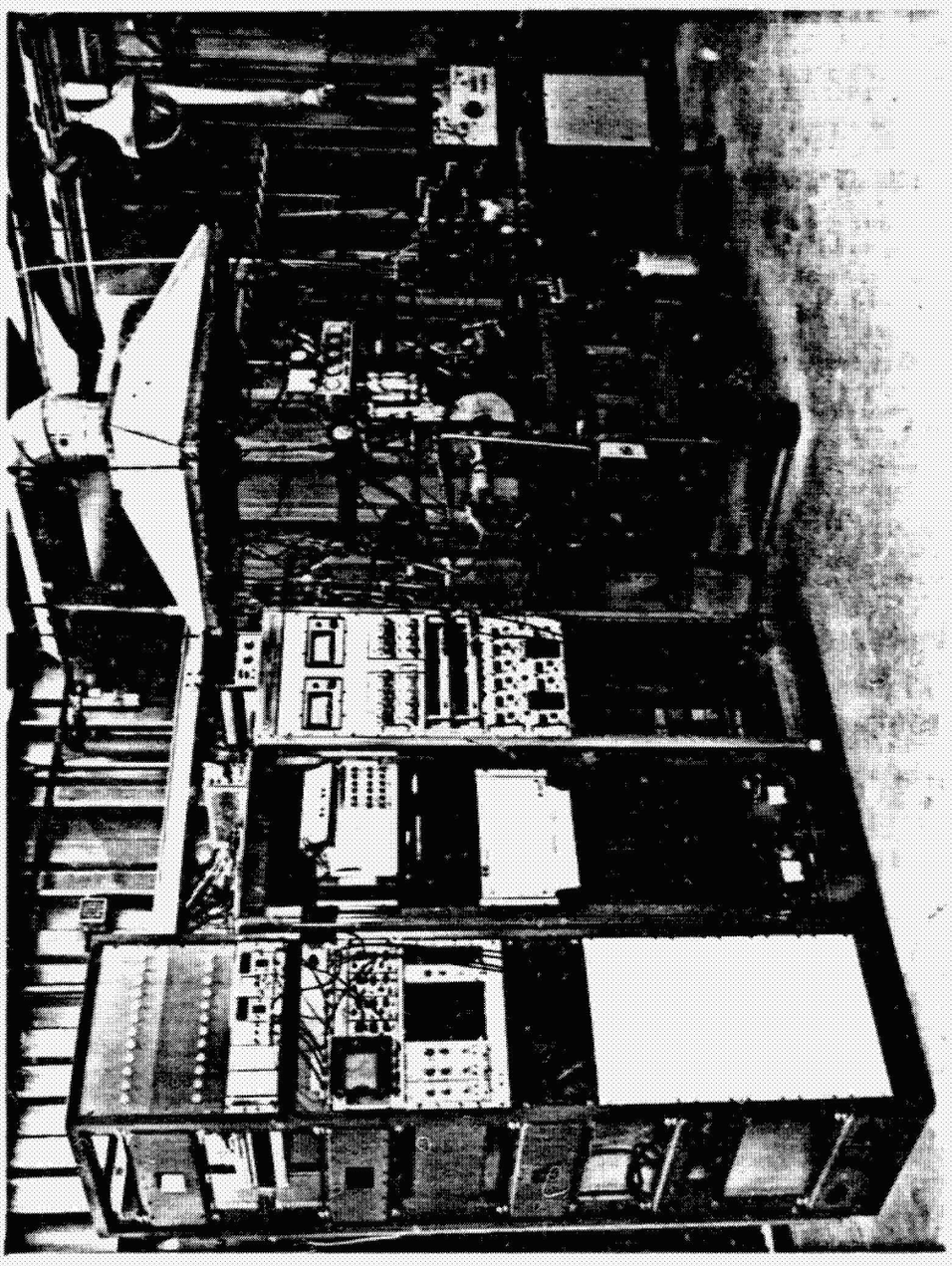

Figure 3. - GPU 3 test setup.

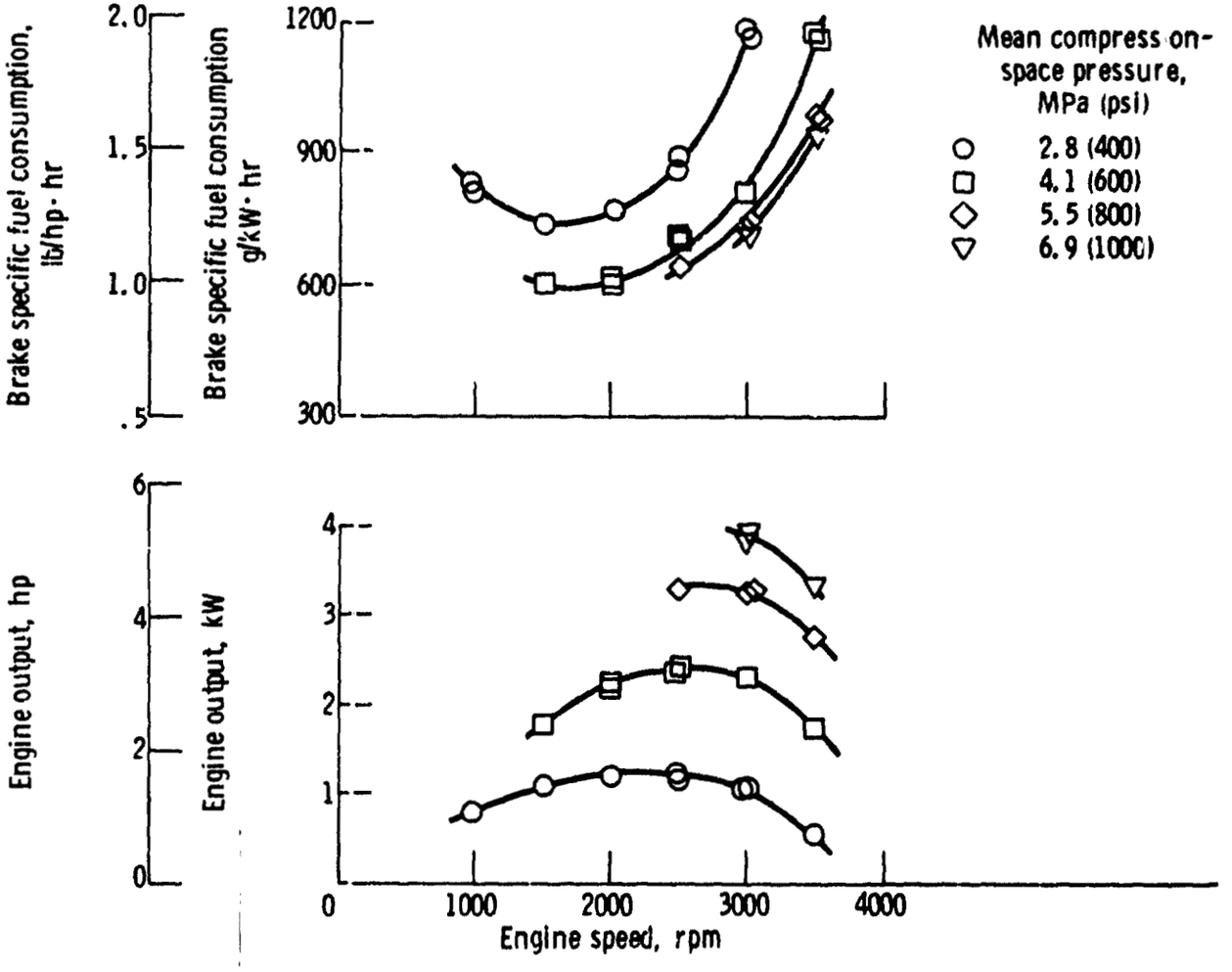

Figure 4. - Helium engine performance as function of engine speed and mean compression-space pressure for a heater-tube gas temperature of 650° C (1200° F). Water inlet temperature, 13° C (56° F).

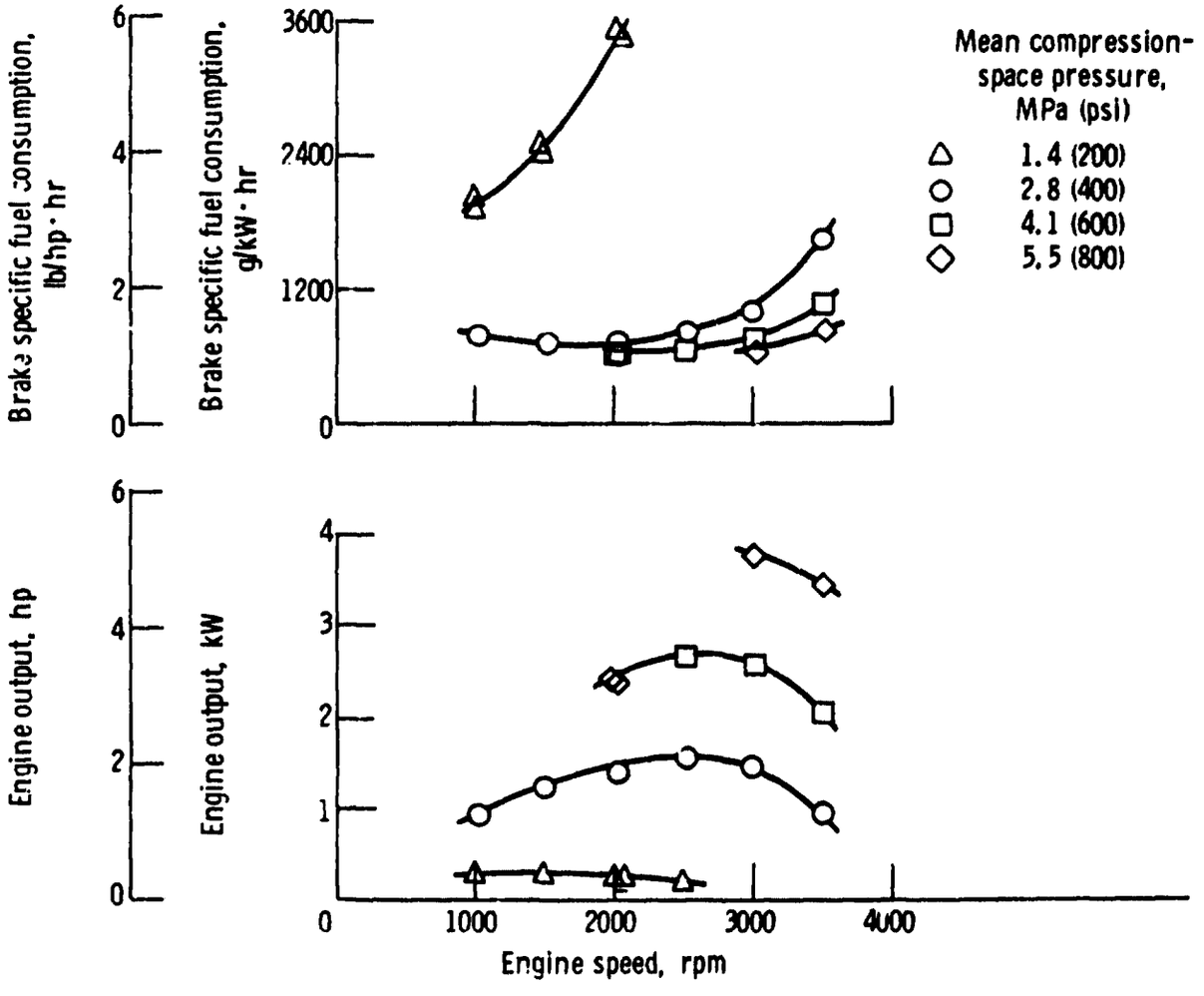

Figure 5. - Helium engine performance as function of engine speed and mean compression-space pressure for heater-tube gas temperature of 705° C (1300° F). Water inlet temperature, 13° C (56° F).

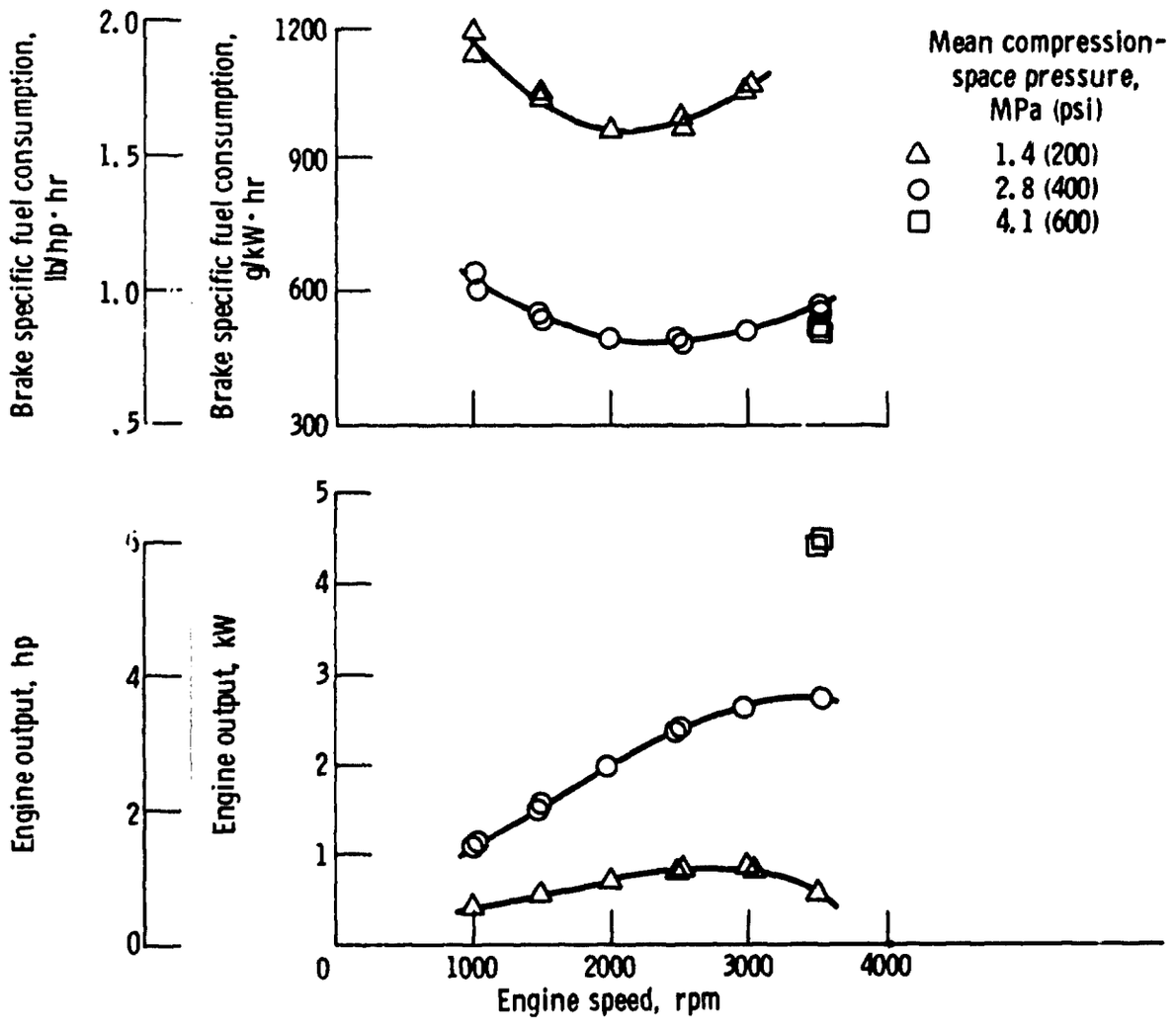

Figure 6. - Hydrogen engine performance as function of engine speed and mean compression-space pressure for heater-tube gas temperature of 705° C (1300° F). Water inlet temperature, 15° C (59° F).

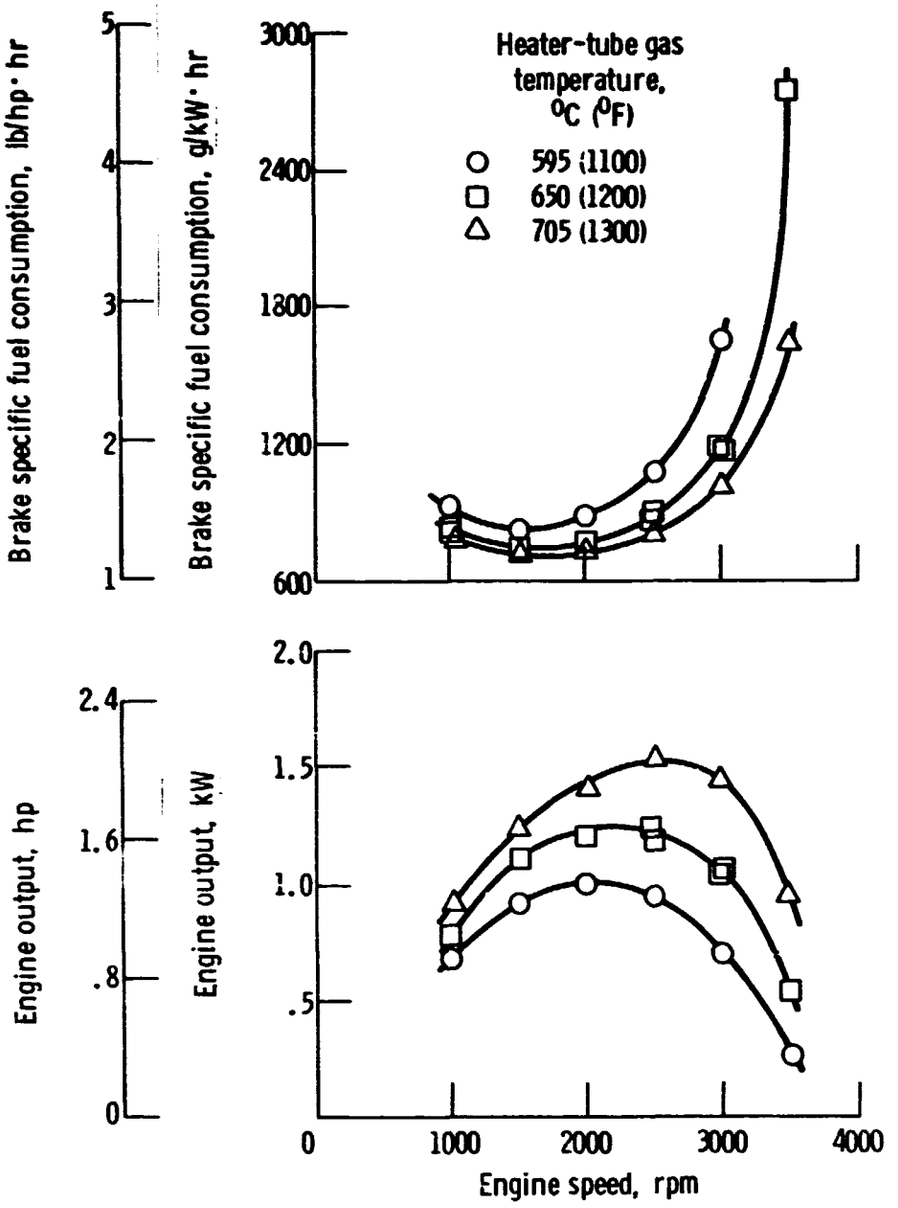

Figure 7. - Helium engine performance as function of engine speed and heater-tube gas temperature for mean compression-space pressure of 2.8 MPa (400 psi). Water inlet temperature, 13° C (56° F).

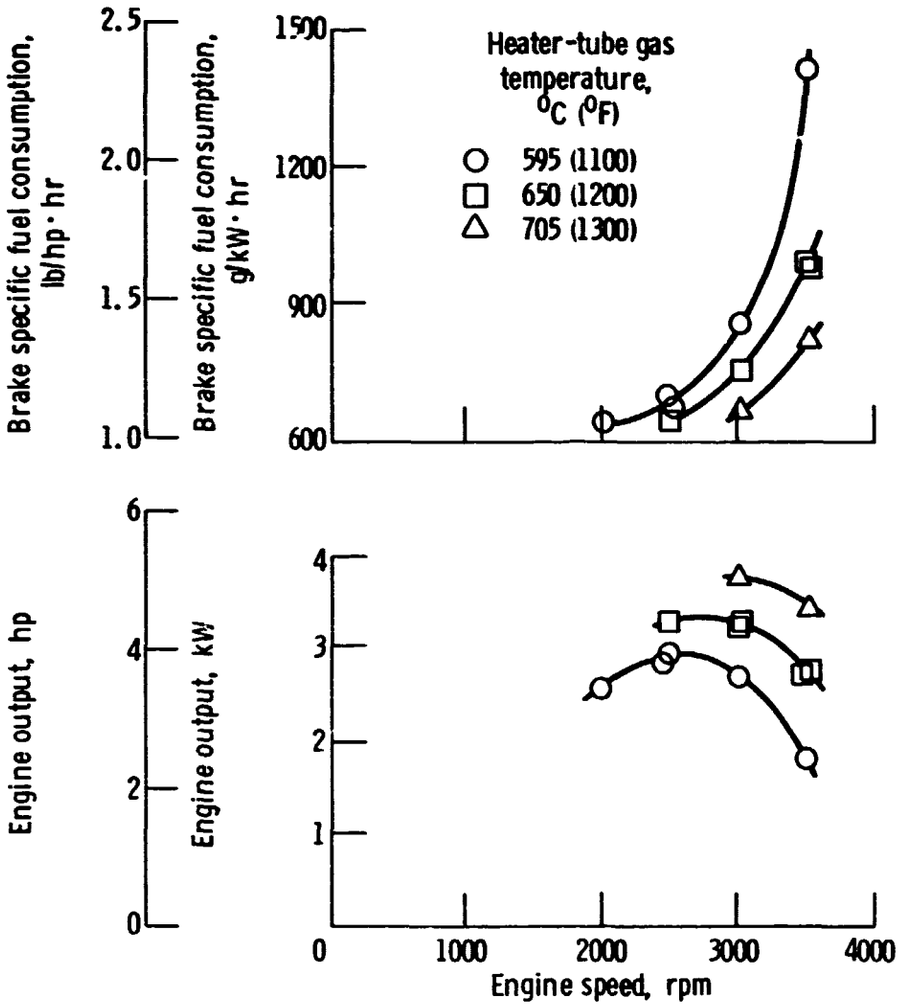

Figure 8. - Helium engine performance as function of engine speed and heater-tube gas temperature for mean compression-space pressure of 5.5 MPa (800 psi). Water inlet temperature, 13° C (56° F).

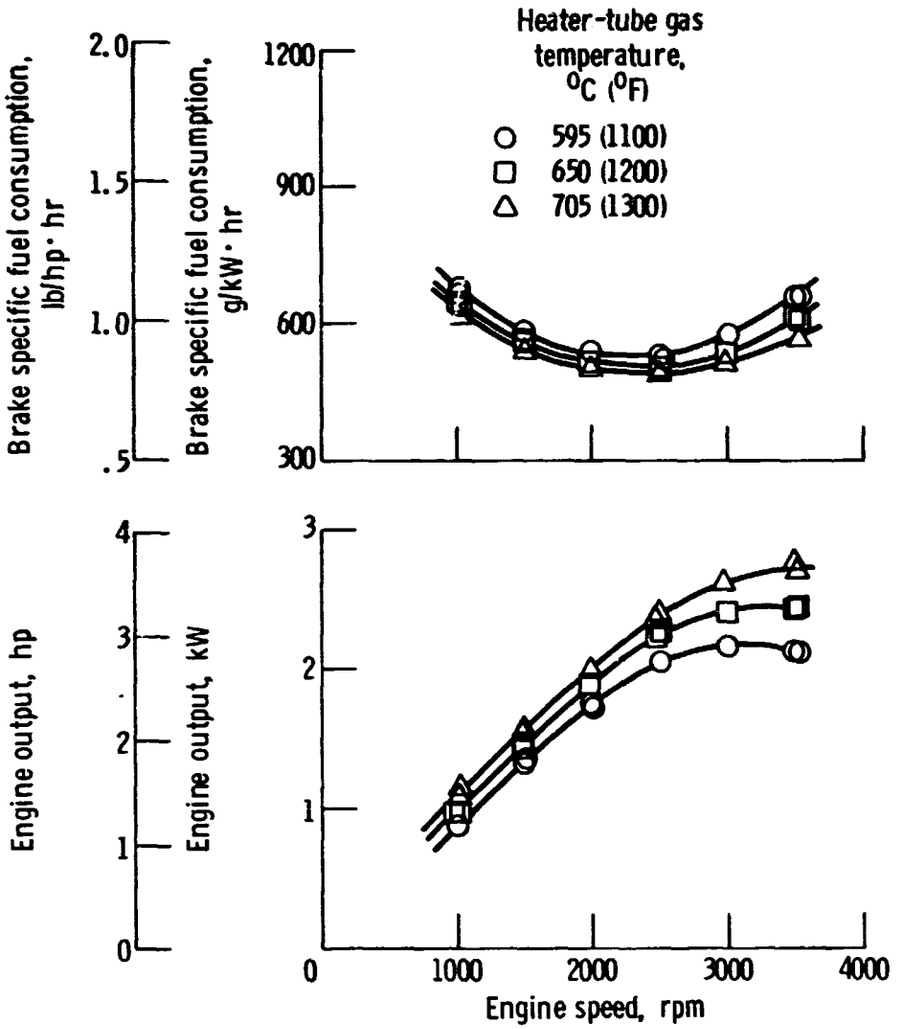

Figure 9. - Hydrogen engine performance as function of engine speed and heater-tube gas temperature for mean compression-space pressure of 2.8 MPa (400 psi). Water inlet temperature, 15° C (59° F).

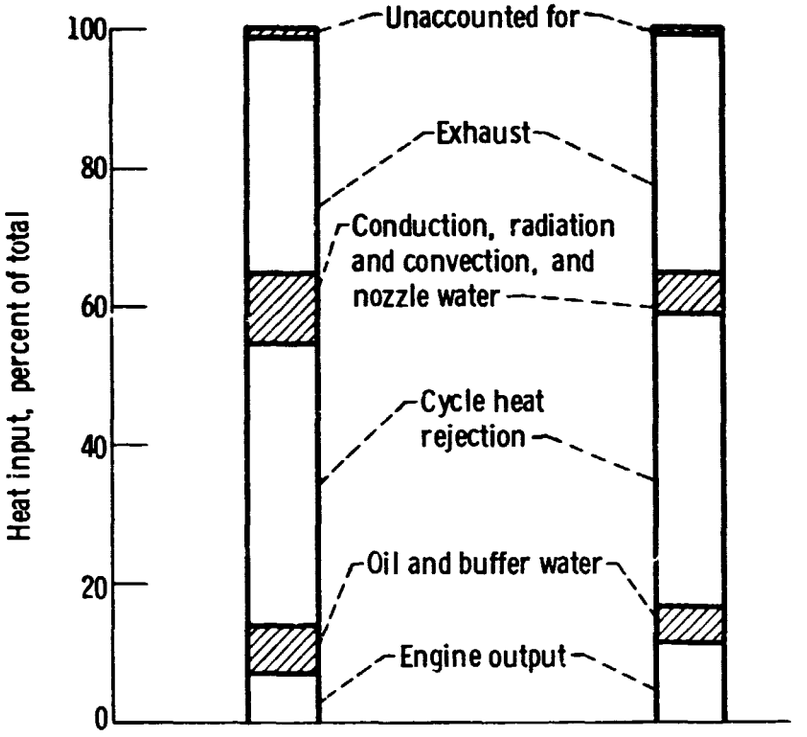

Engine output, kW (hp):	1.05 (1.4)	3.9 (5.2)
Mean compression-space pressure, MPa (psi):	2.8 (400)	6.9 (1000)

Figure 10. - Energy balances for two mean compression-space pressures. Working fluid, helium; heater-tube gas temperature, 650° C (1200° F); engine speed, 3000 rpm.

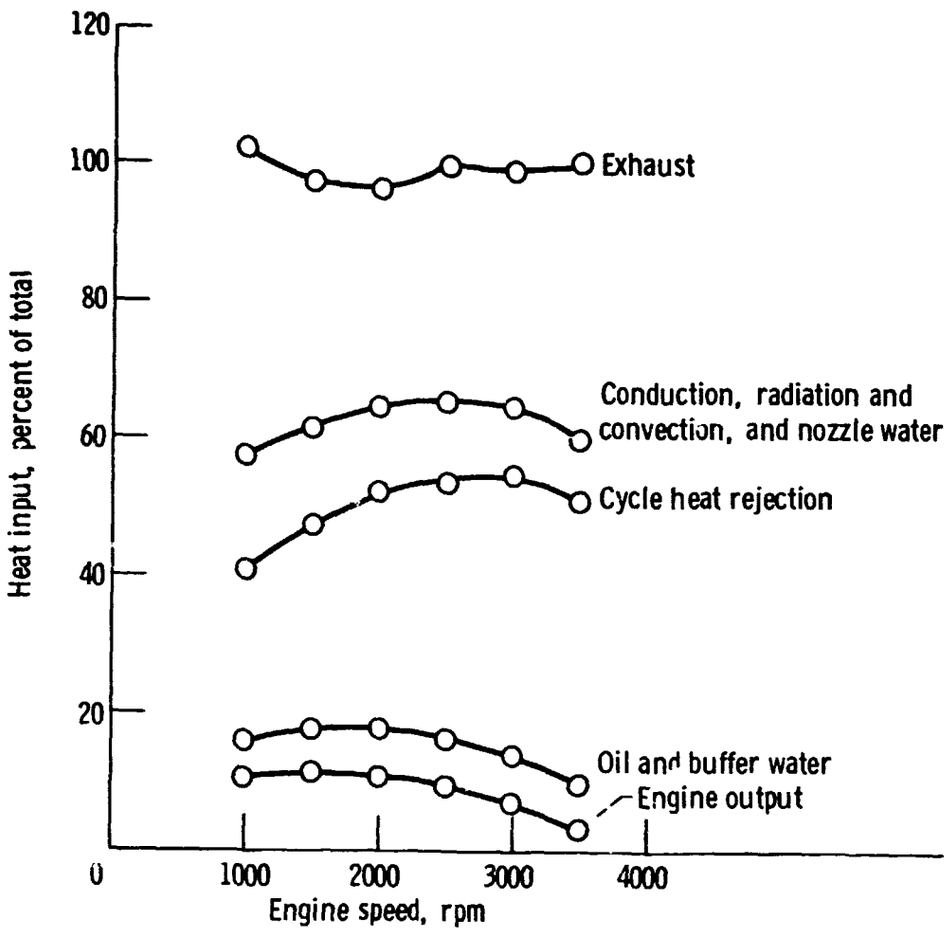

Figure 11. - Energy balance as function of engine speed. Working fluid, helium; heater-tube gas temperature, 650° C (1200° F); mean compression-space pressure, 2.8 MPa (400 psi).

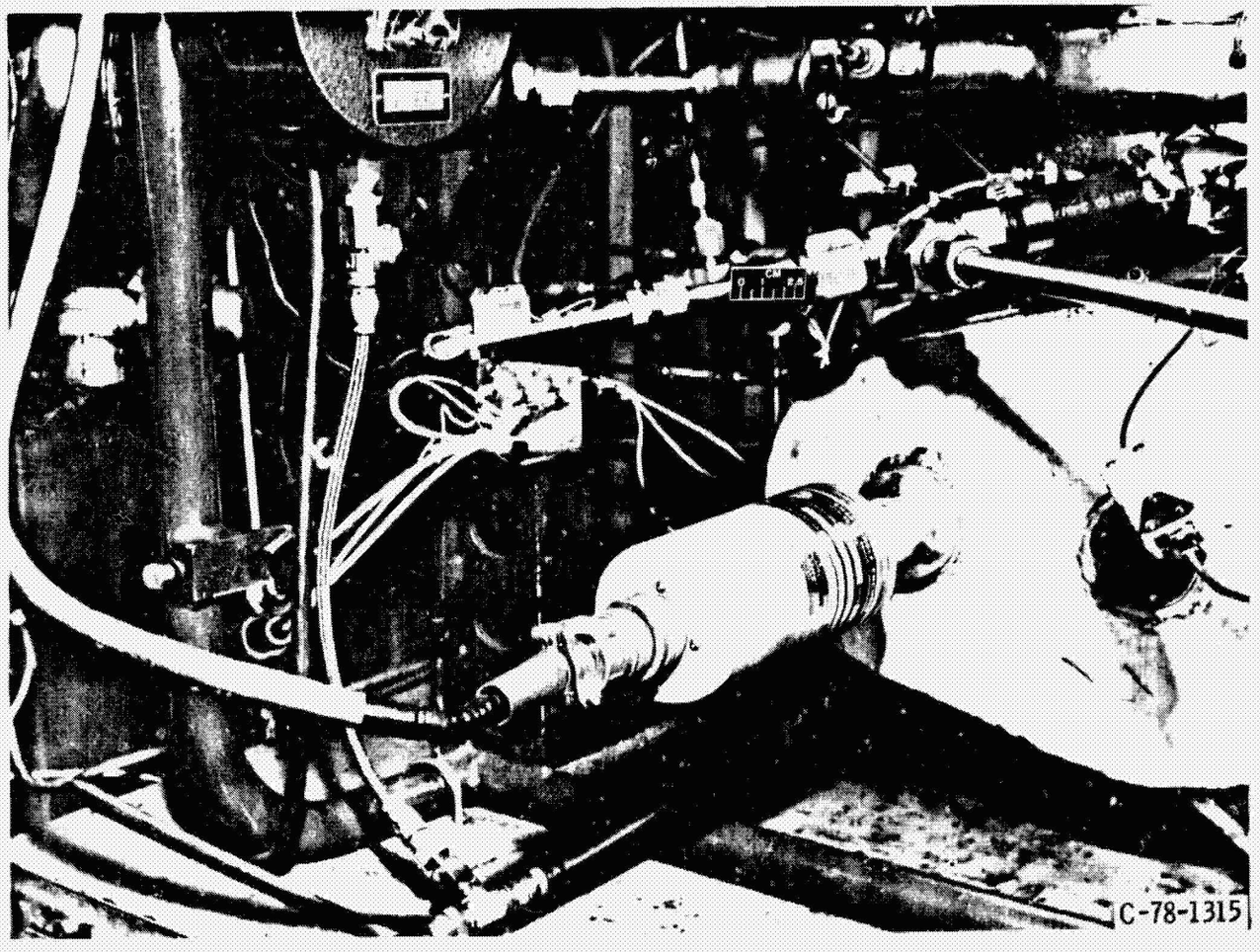

Figure 12. - Crankshaft-angle encoder.

REPRODUCIBILITY OF THE
ORIGINAL PAGE IS POOR

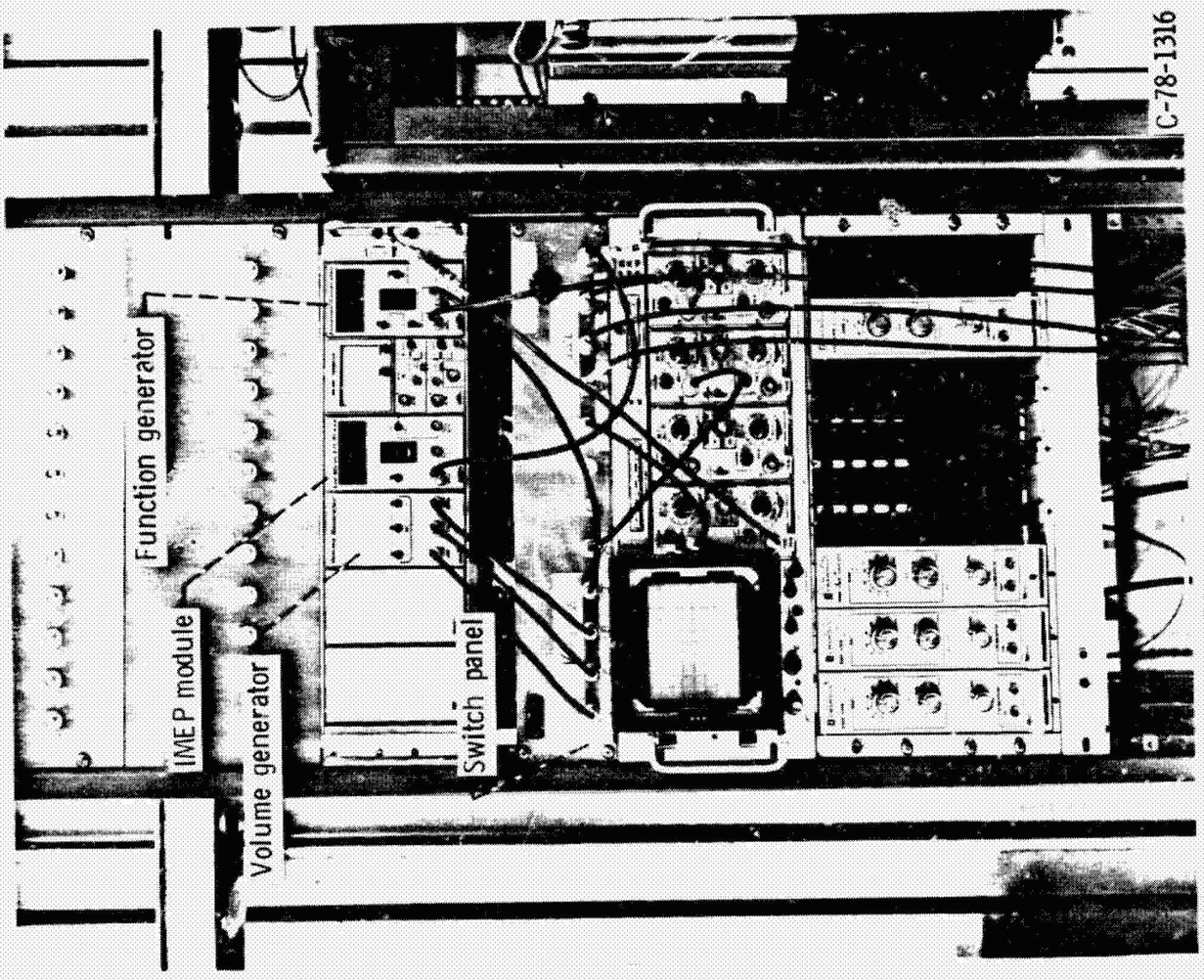

Figure 13. - Pressure-volume recording system.

REPRODUCIBILITY OF THE
ORIGINAL PAGE IS POOR

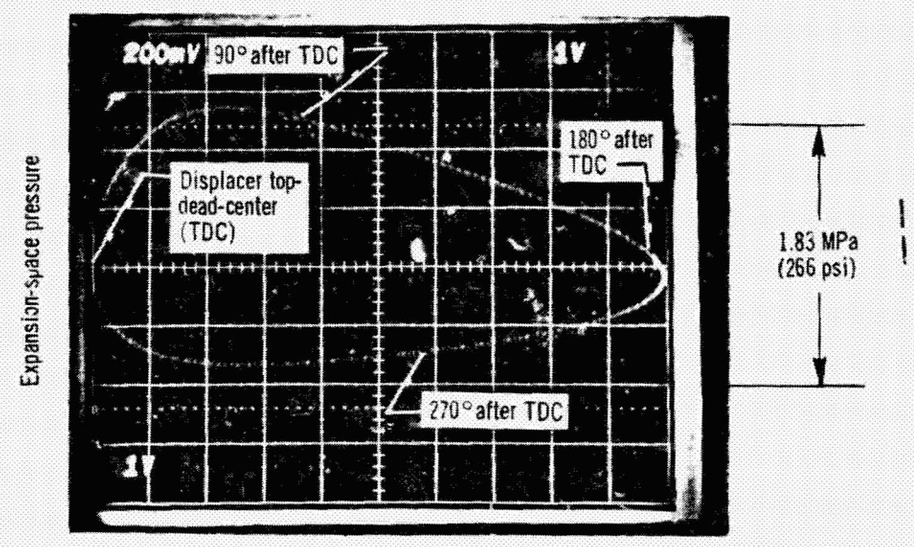

(a) Expansion space - output, 7.98 kW (10.69 hp).

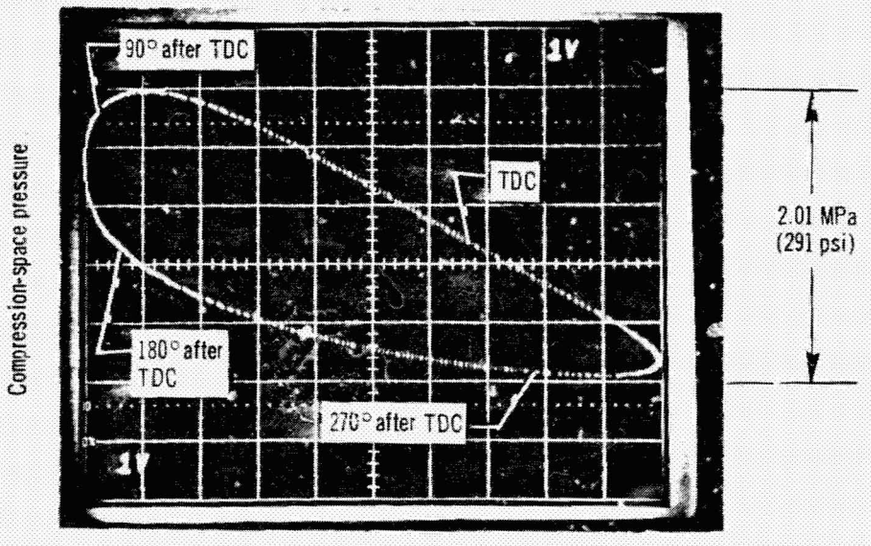

(b) Compression space - output, 5.67 kW (7.59 hp).

Figure 14. - Helium pressure-volume diagrams. Heater-tube gas temperature, 650° C (1200° F); engine output, 1.05 kW (1.42 hp); mean compression-space pressure, 2.8 MPa (400 psi); engine speed, 2995 rpm.

REPRODUCIBILITY OF THE
ORIGINAL PAGE IS POOR

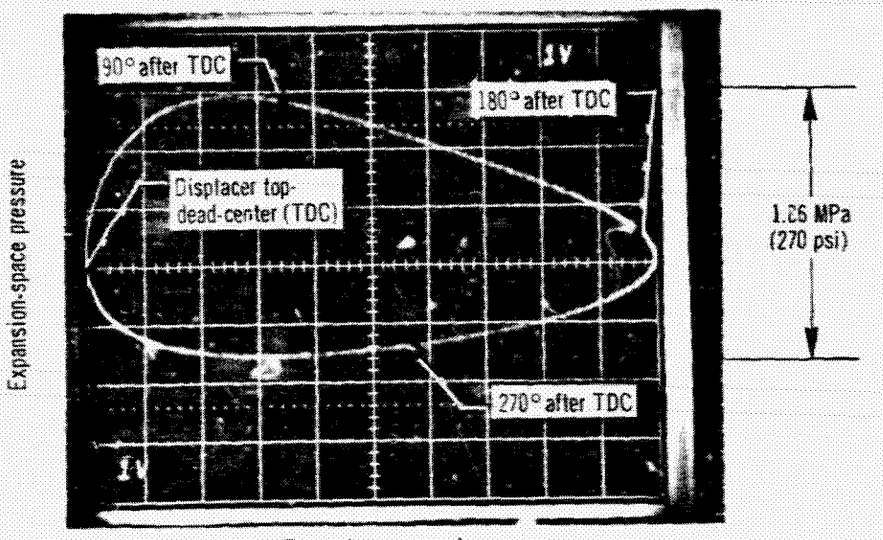

(a) Expansion space - output, 8.18 kW (10.96 hp).

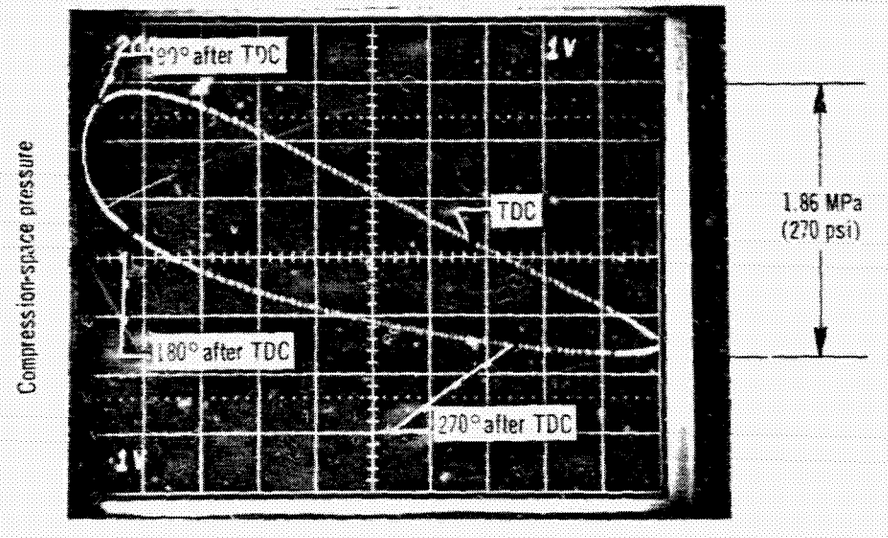

(b) Compression space - output, 4.71 kW (6.31 hp).

Figure 15. - Hydrogen pressure-volume diagrams. Heater-tube gas temperature, 650° C (1200° F); engine output, 2.41 kW (3.23 hp); mean compression-space pressure, 2.8 MPa (400 psi); engine speed, 2990 rpm.

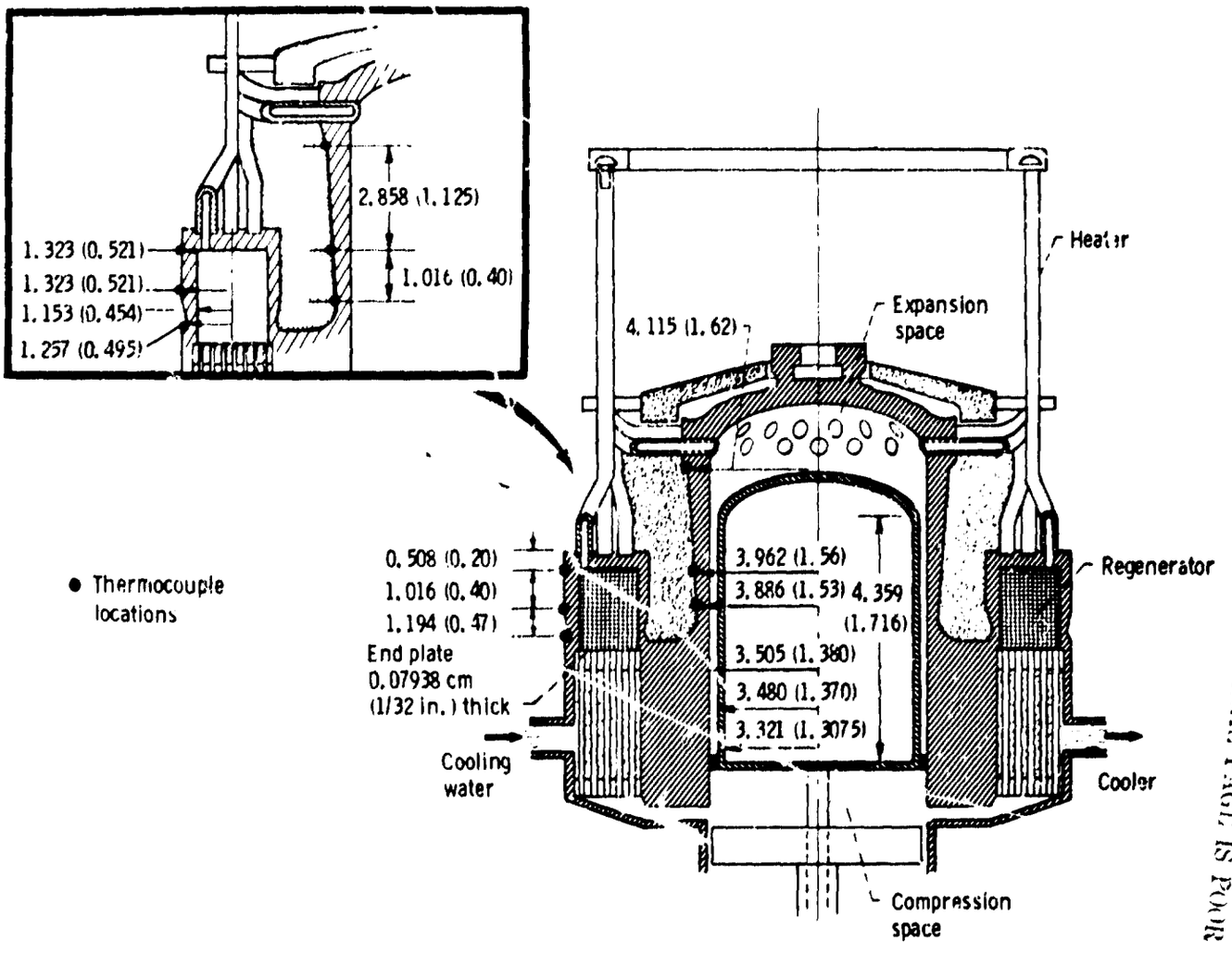

Figure 16. - Schematic showing dimensions needed for calculating heat conduction. (Regenerator housings, cylinder, and displacer are 310 stainless steel. Dimensions are in cm (in.).)

REPRODUCIBILITY OF THE ORIGINAL PAGE IS POOR

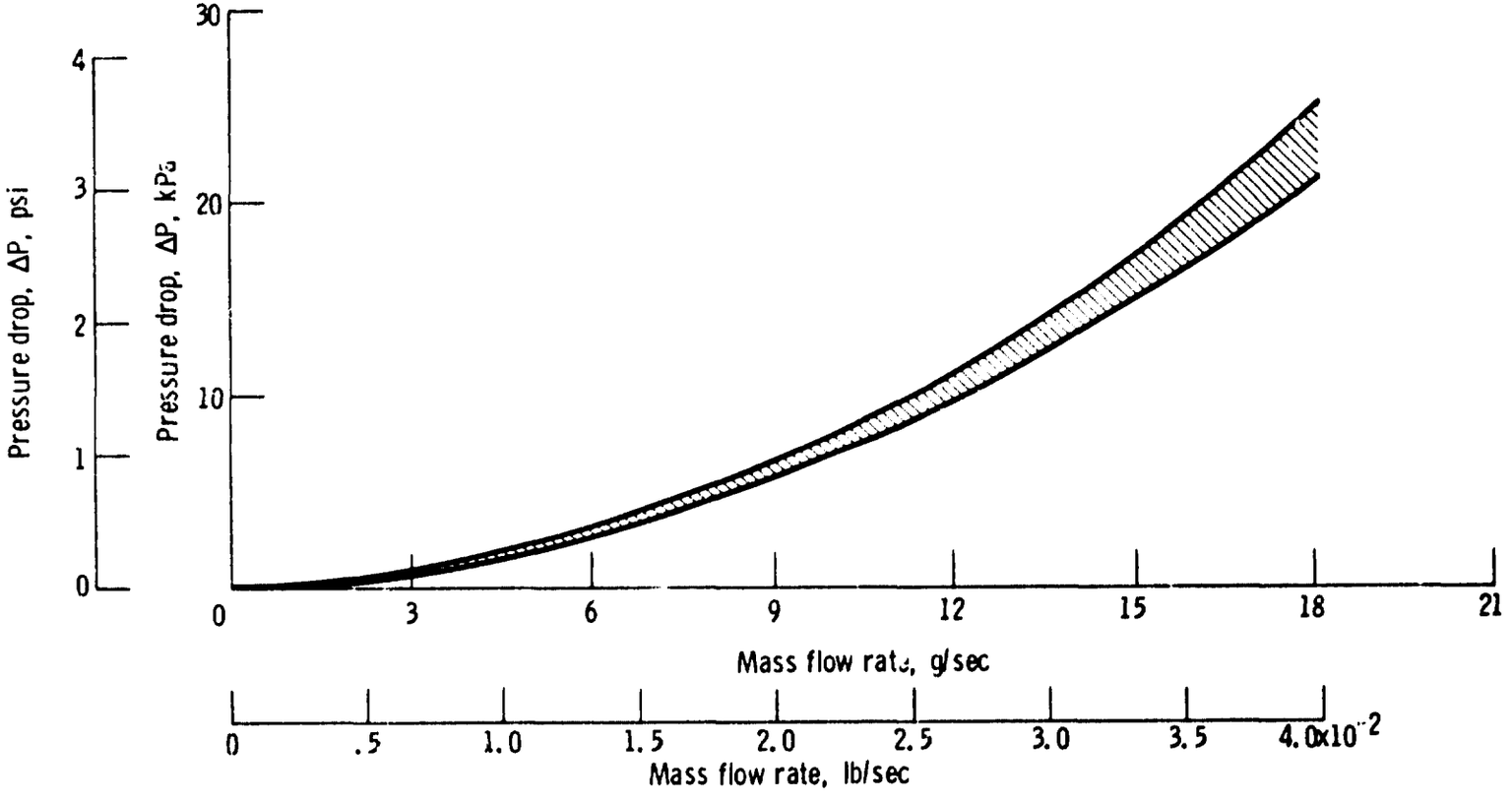

Figure 17. - Range of pressure drop as function of mass flow rate for GPU 3 coolers. (Air at 150-psi inlet; coolers new when tested.)

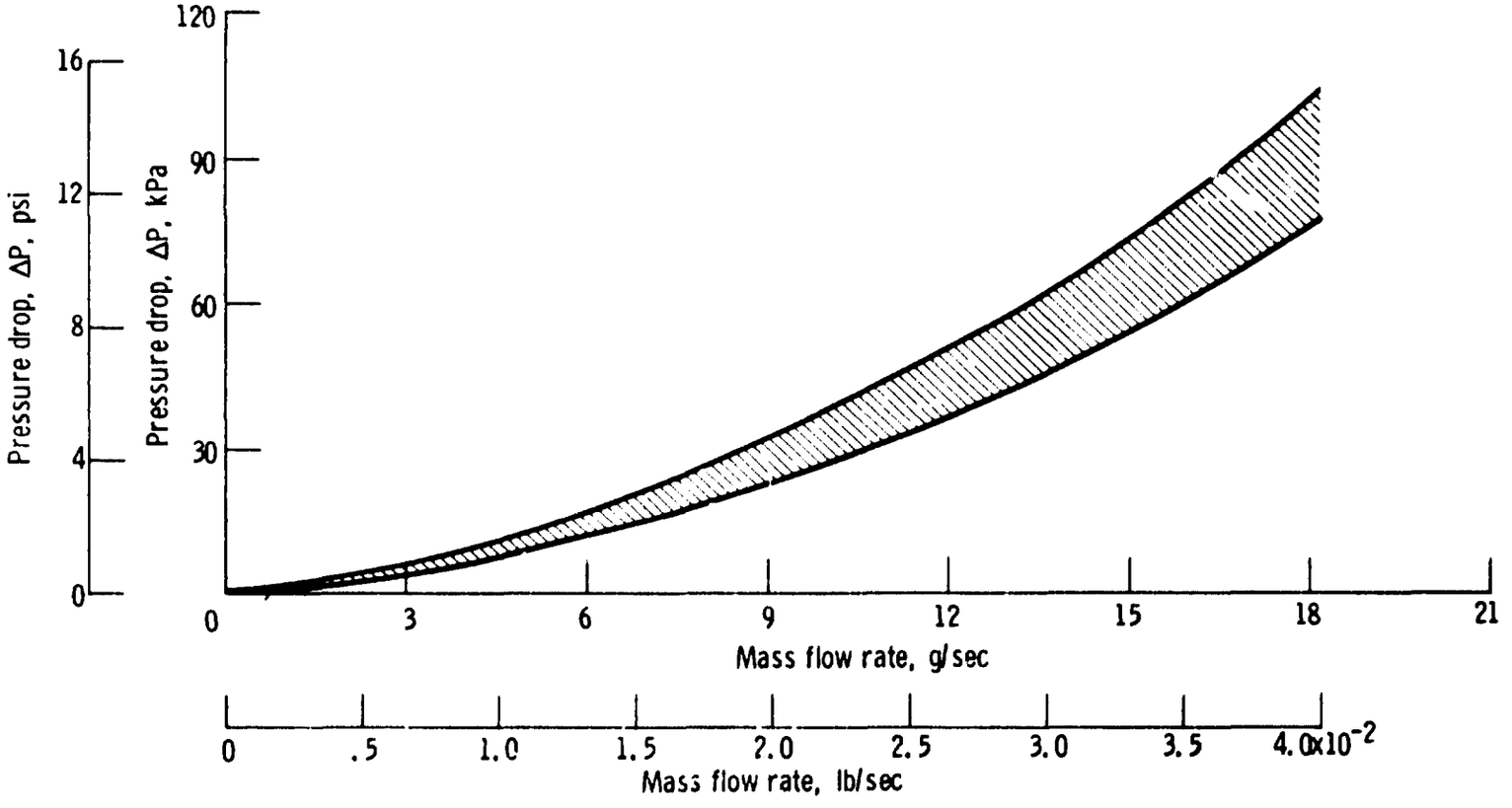

Figure 18. - Range of pressure drop as function of mass flow rate for GPU 3 regenerators. (Air at 150-psi inlet; regenerators new when tested.)

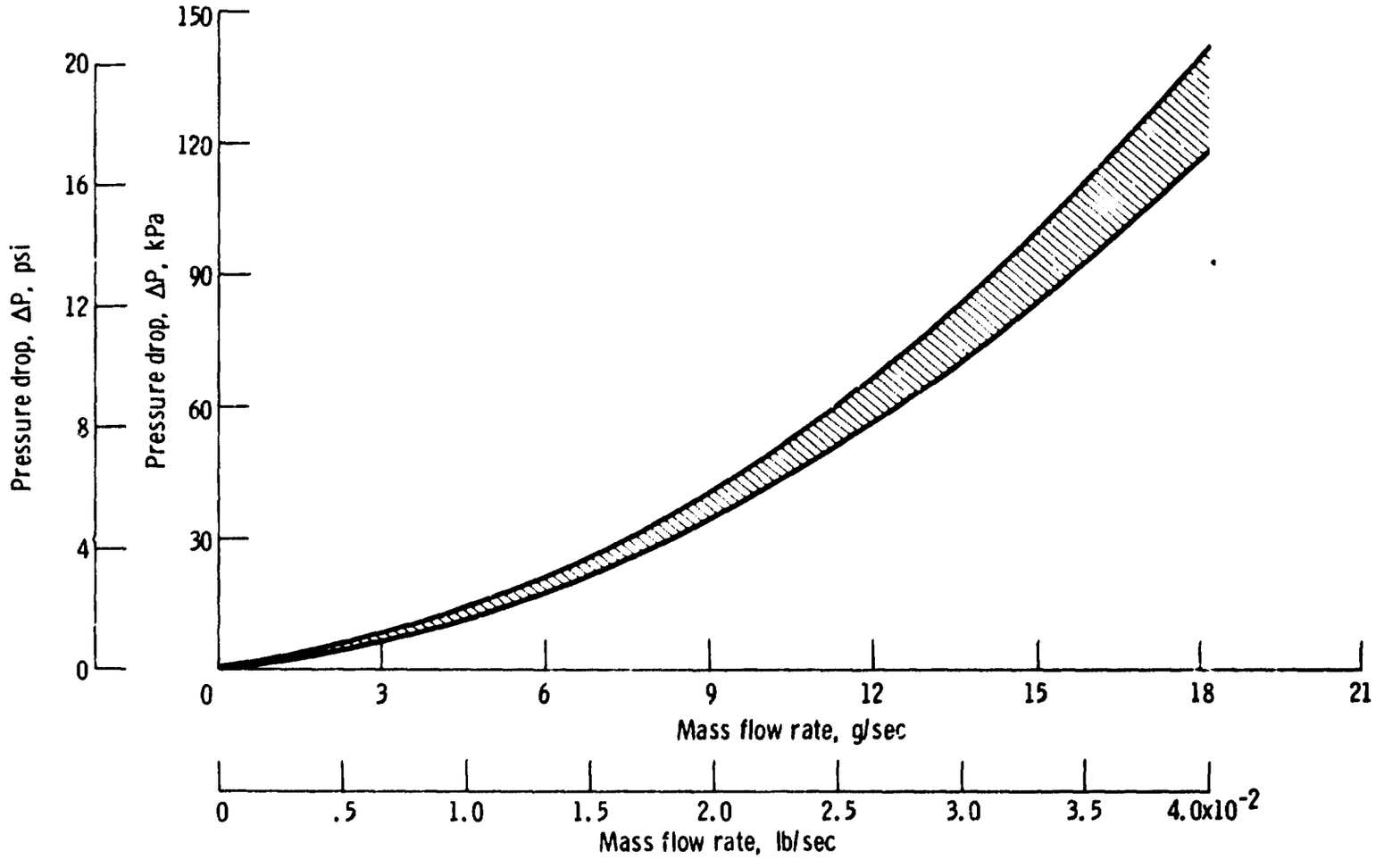

Figure 19. - Range of pressure drop as function of mass flow rate for GPU 3 cooler-regenerator cartridges. (Air at 150-psi inlet; cartridges new when tested.)

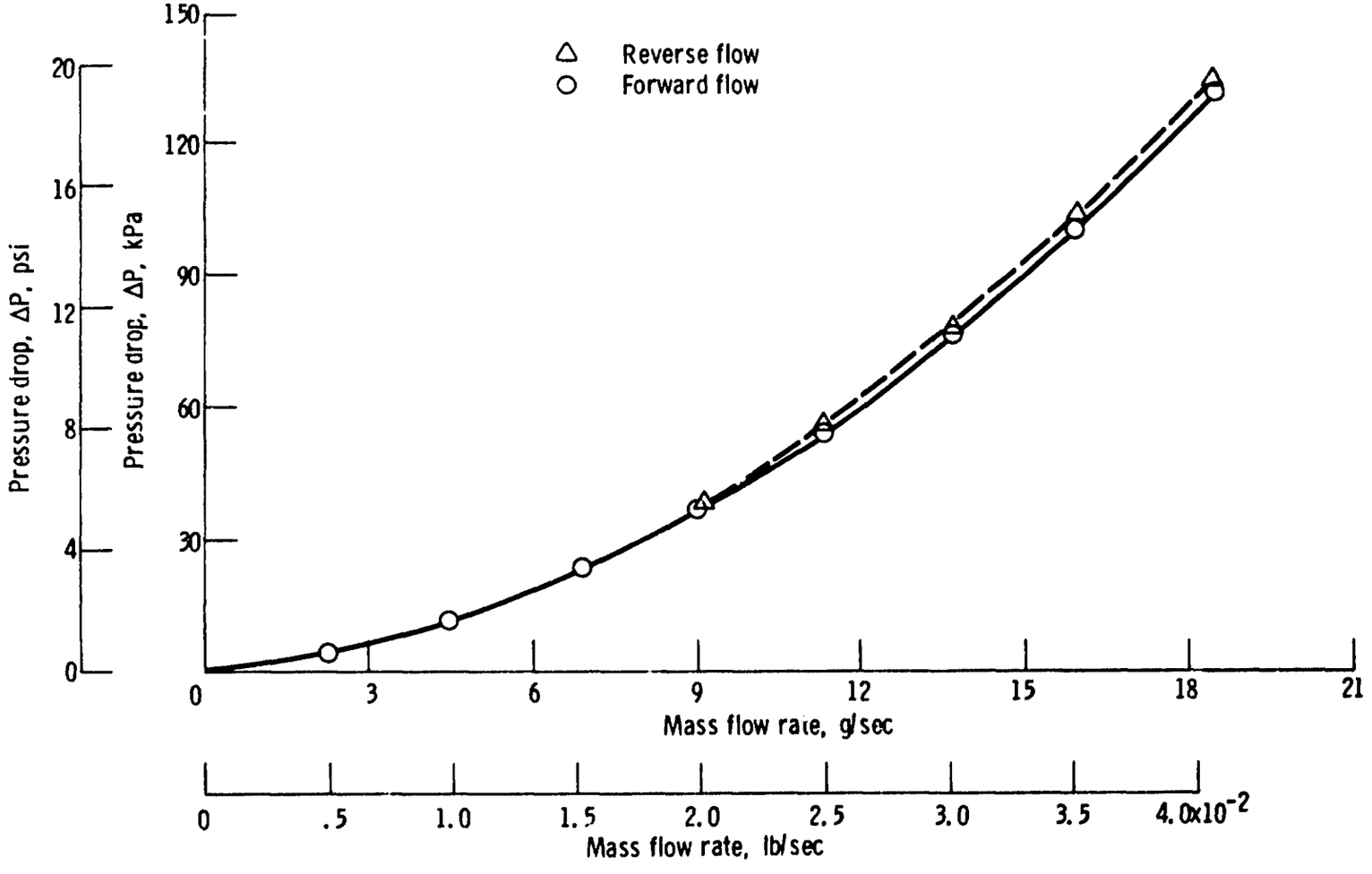

Figure 20. - Pressure drop as function of mass flow rate for typical GPU 3 cooler-regenerator cartridge - forward and reverse flow. (Air at 150-psi inlet; cartridge new when tested; forward flow is flow from cooler to regenerator.)

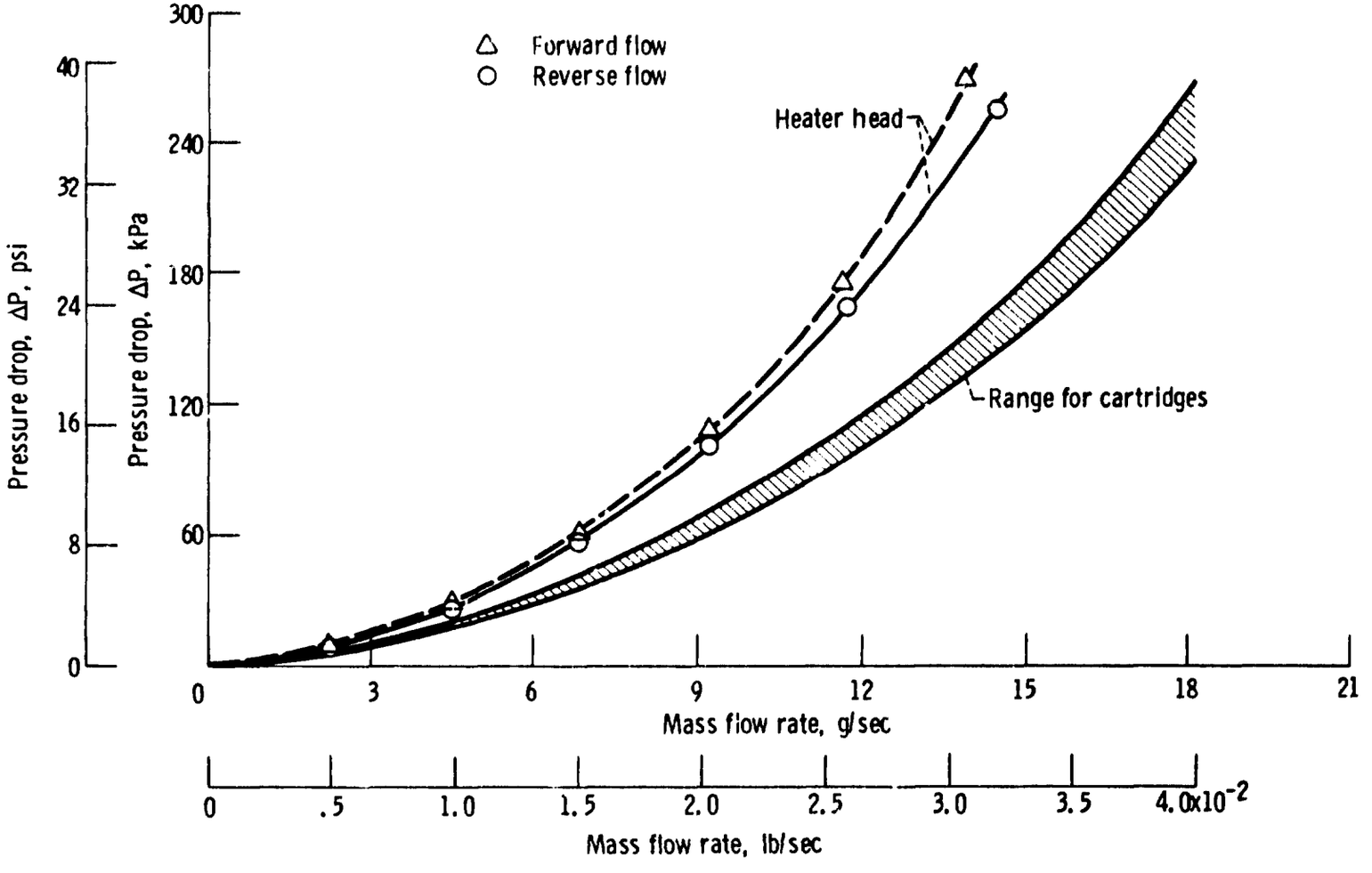

Figure 21. - Pressure drop as function of mass flow rate for heater head and for cooler-regenerator cartridges. (Air at 115-psi inlet; 80-hr run time on cartridges; forward flow is flow from compression space to expansion space.)

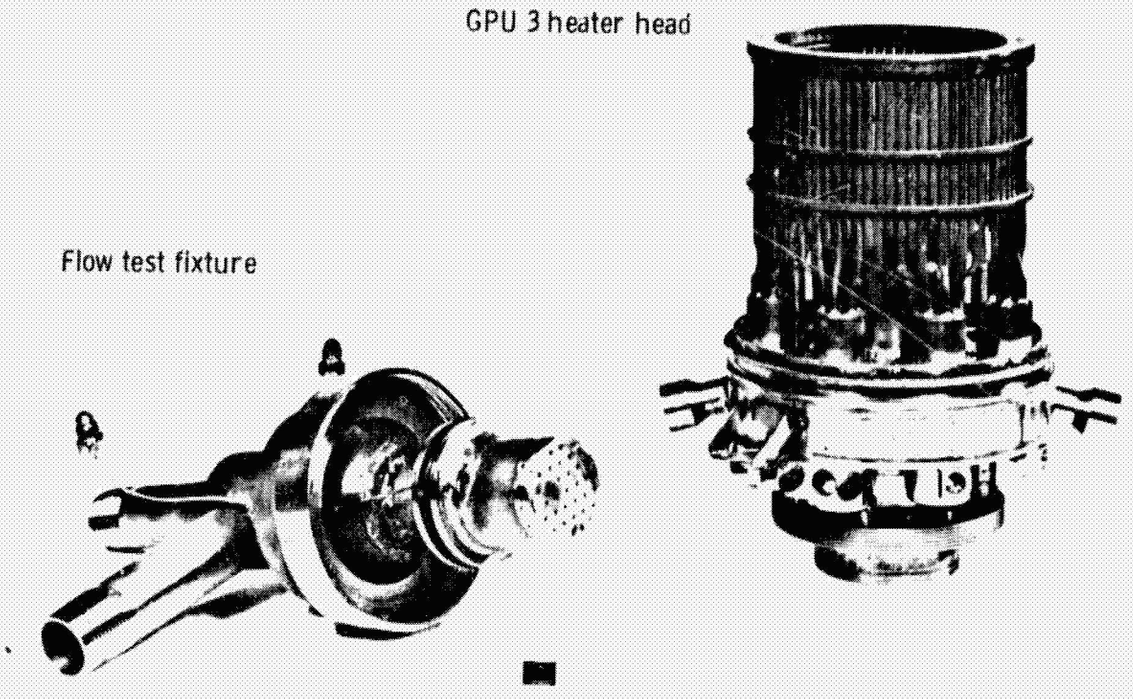

C-78-3943

Figure 22. - Steady-state flow test fixture for GPU 3 heater head.

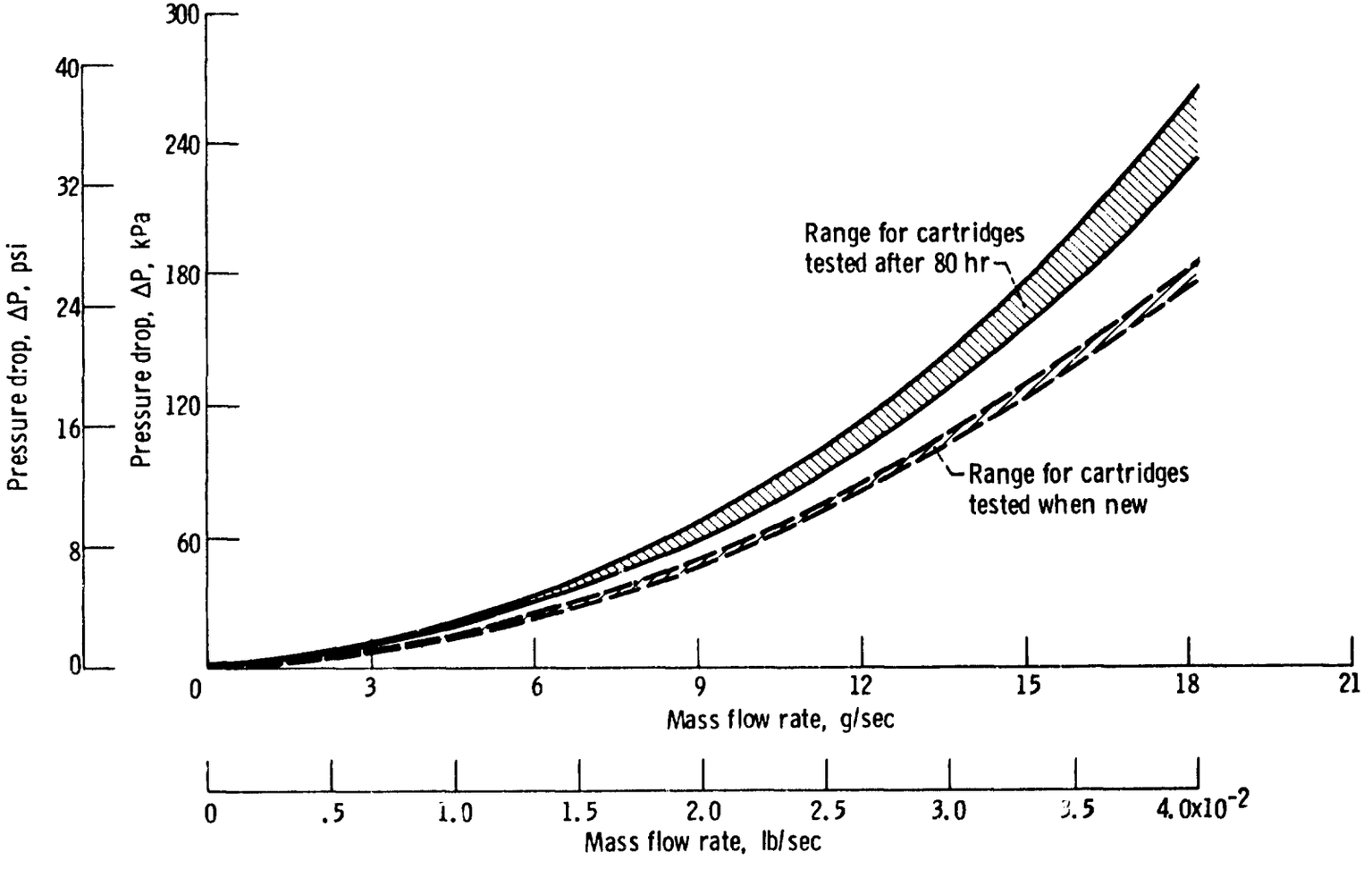

Figure 23. - Pressure drop as function of mass flow rate for GPU 3 cooler-regenerator cartridges when new and after 80 hours of testing. (Air at 115-psi inlet; data for forward flow only.)

REPRODUCIBILITY OF THE ORIGINAL PAGE IS POOR

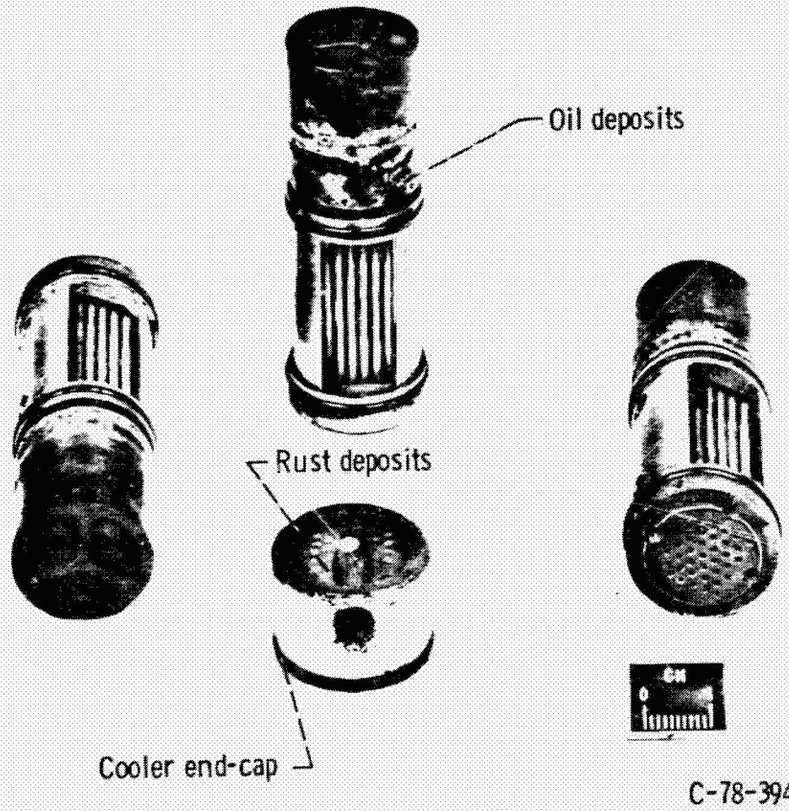

Figure 24. - GPU 3 cooler-regenerator cartridges after 80 hours of testing.

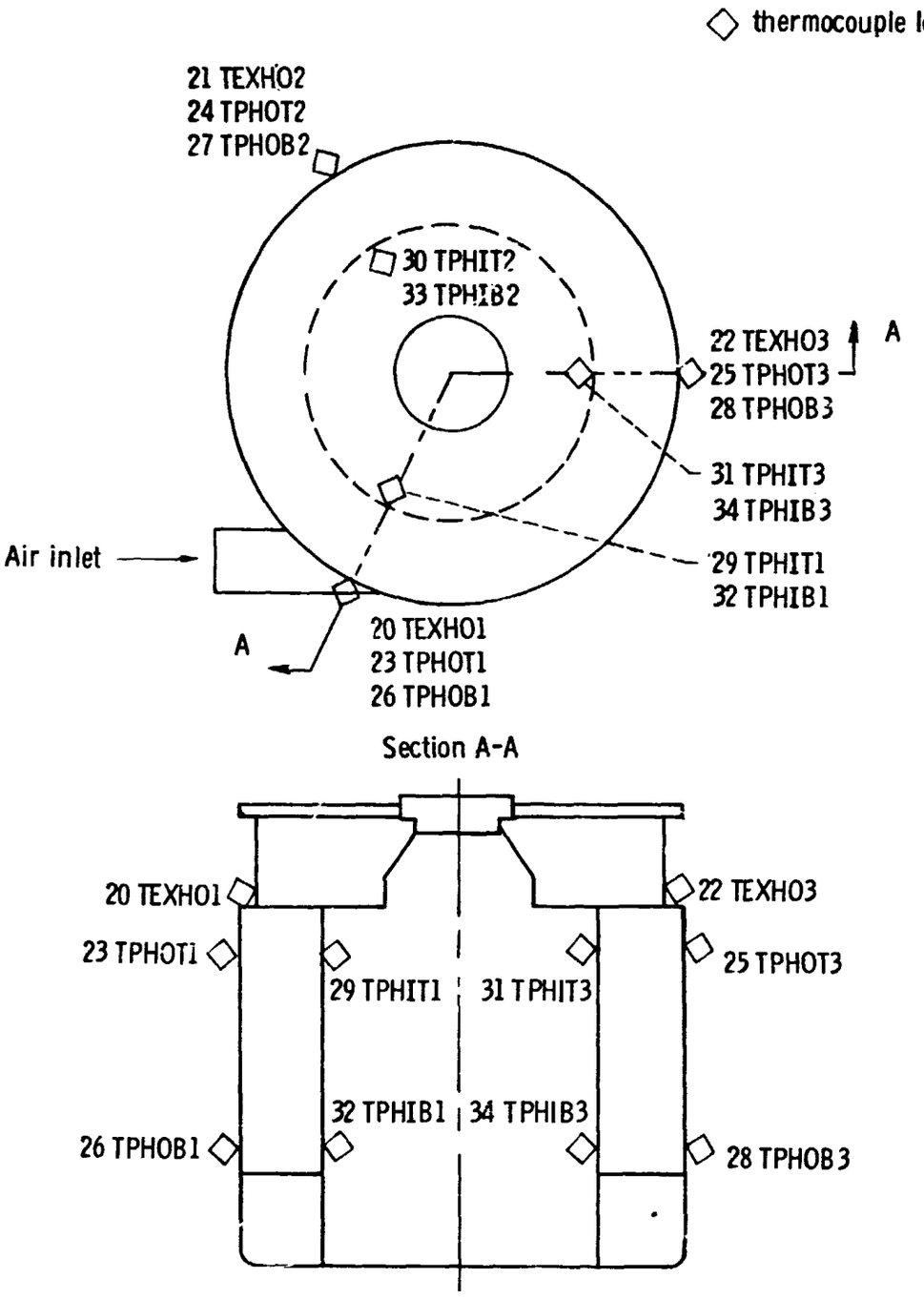

Figure 25. - GPU 3 preheater thermocouple locations.

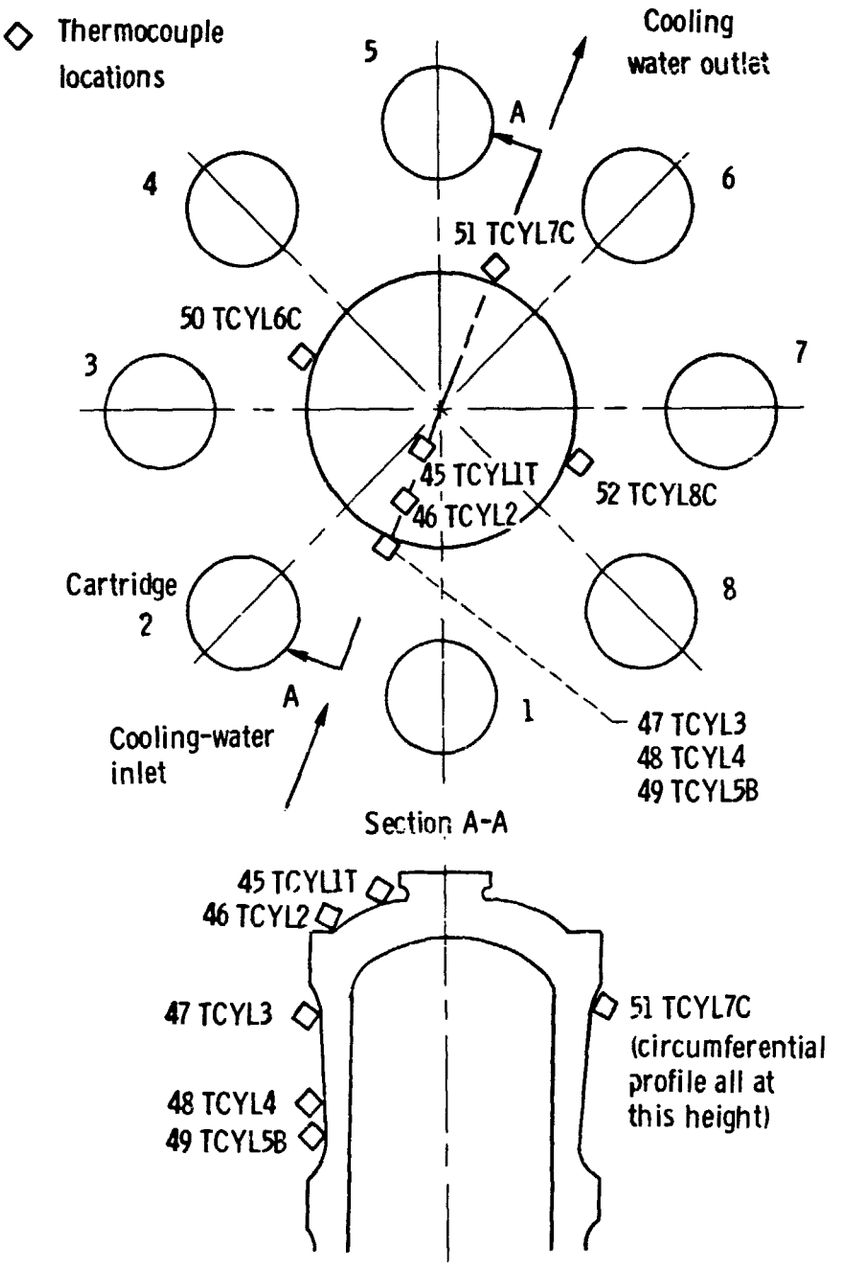

Figure 26. - GPU 3 cylinder thermocouple locations.

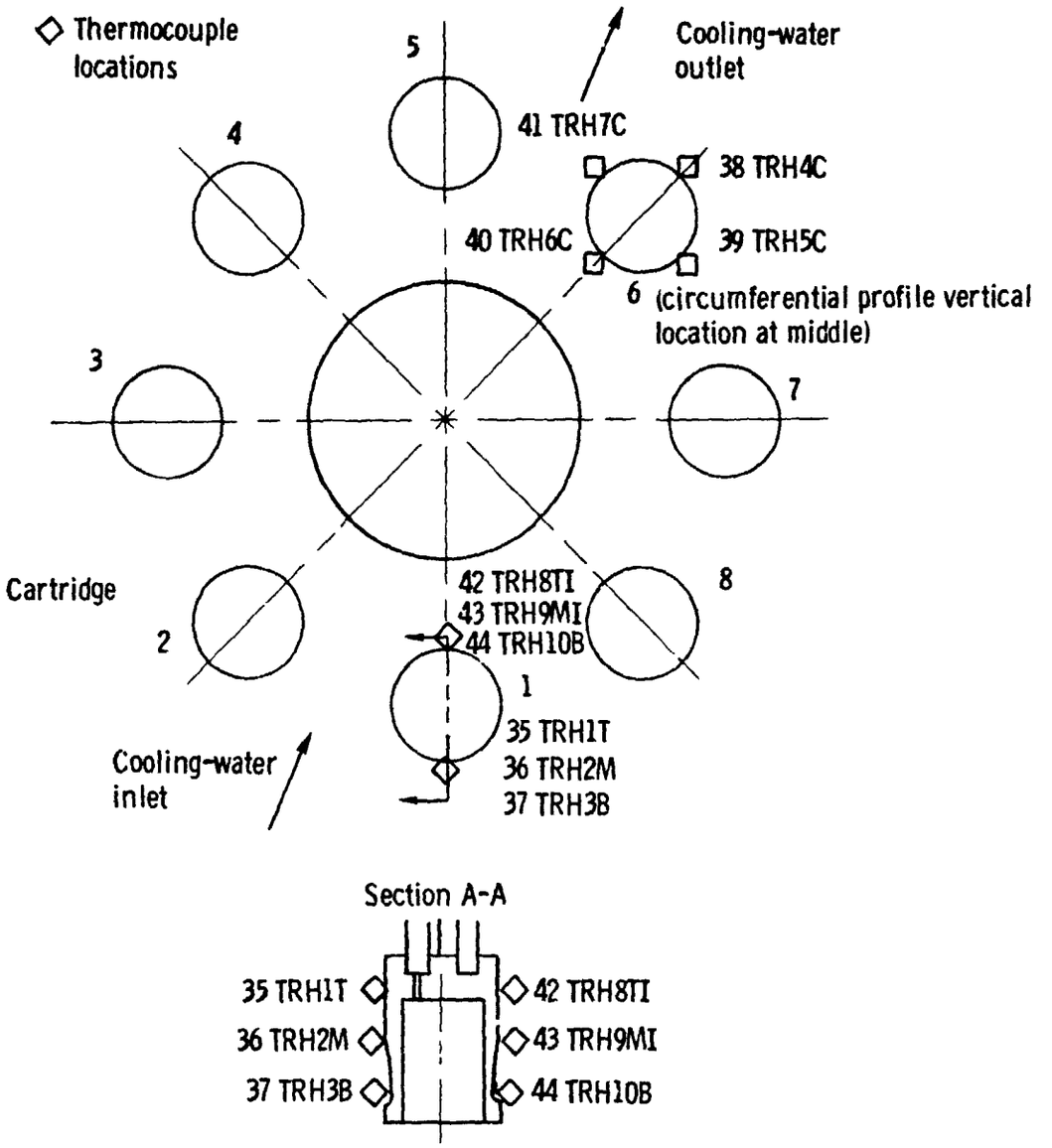

Figure 27. - GPU 3 regenerator housing thermocouple locations.

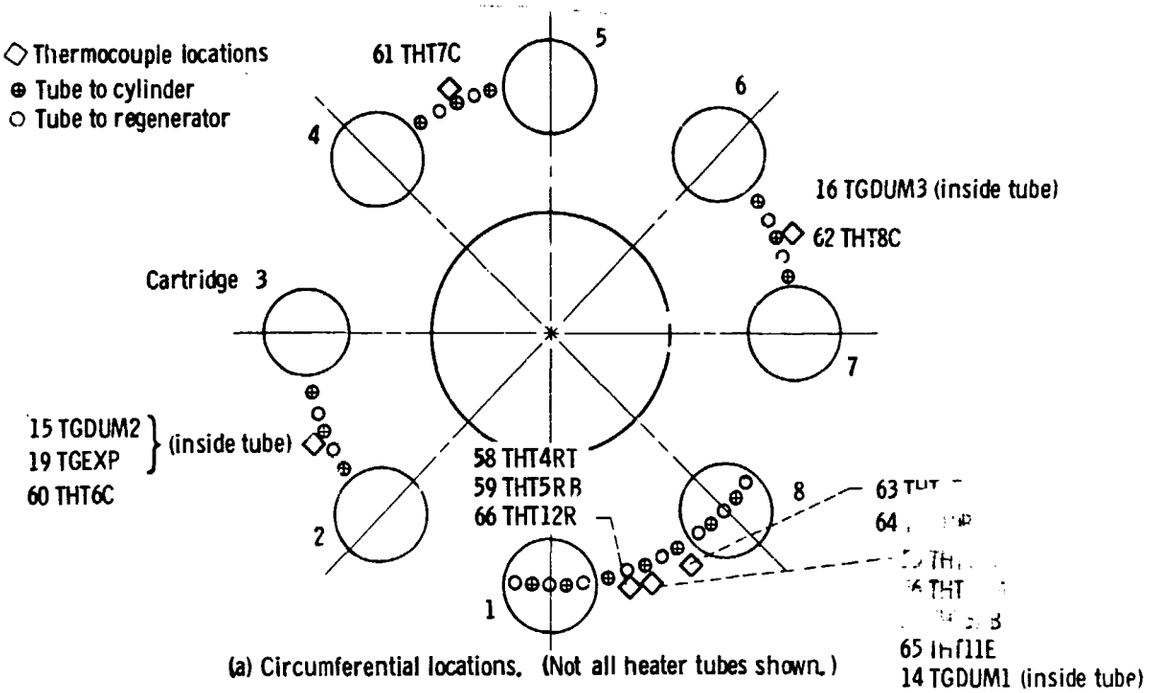

(a) Circumferential locations. (Not all heater tubes shown.)

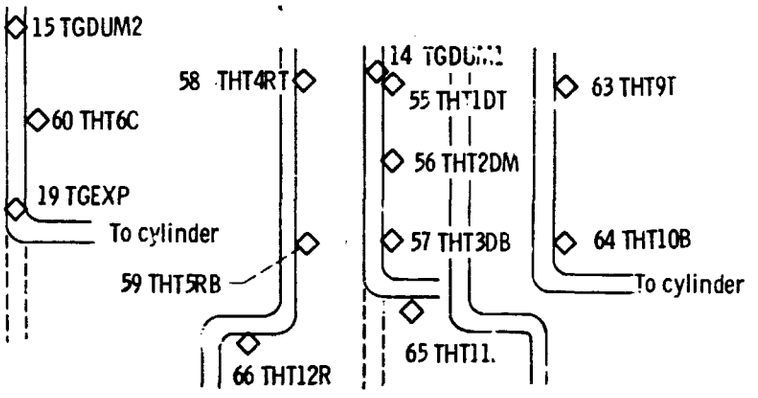

(b) Vertical locations.

Figure 28. - GPU 3 heater-tube and heater-tube gas thermocouple locations.

67

1. Report No.	2. Government Accession No.	3. Recipient's Catalog No.
NASA TM-79103		

4. Title and Subtitle	5. Report Date
LOW-POWER BASELINE TEST RESULTS FOR THE GPU 3 STIRLING ENGINE	April 1979
	6. Performing Organization Code

7. Author(s)	8. Performing Organization Report No.
Lanny G. Thieme	E-9927
	10. Work Unit No.

9. Performing Organization Name and Address	11. Contract or Grant No.
National Aeronautics and Space Administration Lewis Research Center Cleveland, Ohio 44135	
	13. Type of Report and Period Covered
12. Sponsoring Agency Name and Address	Technical Memorandum
U.S. Department of Energy Division of Transportation Energy Conservation Washington, D.C. 20545	14. Sponsoring Agency ~~Code~~ Report No. DOE/NASA/1040-79/6

15. Supplementary Notes

Final report. Prepared under Interagency Agreement EC-77-A-31-1040.

16. Abstract

As part of its project management responsibilities for the Department of Energy's Stirling Engine Highway Vehicle Systems Program, the NASA Lewis Research Center has converted a 7.5-kW (10-hp) Stirling engine to a research configuration in order to obtain data for validating Stirling-cycle computer simulations. The engine was originally built by General Motors Research Laboratories for the U.S. Army in 1965 as part of a 3-kW engine-generator set that was designated the GPU 3 (Ground Power Unit 3). This report summarizes test results for a range of heater-tube gas temperatures, mean compression-space pressures, and engine speeds with both helium and hydrogen as the working fluid. An instrumentation system to determine indicated work is described and preliminary results are presented.

17. Key Words (Suggested by Author(s))	18. Distribution Statement
Heat engine Stirling engine Stirling cycle Performance data	Unclassified - unlimited STAR Category 85 DOE Category UC-96

19. Security Classif. (of this report)	20. Security Classif. (of this page)	21. No. of Pages	22. Price*
Unclassified	Unclassified		

* For sale by the National Technical Information Service, Springfield, Virginia 22161